Polaris Rocketry: Midterm Report

Brendon Vu (Team Captain)

Nicholas Diamond (Lieutenant Team Captain)

Jordan Akins (Lieutenant Team Captain)

Clarke Dunn

Joshua Lucero

Jonathan Smith

Luna Sawaged

MECH 4045

Professor Douglas Gallagher

Spring 2021

Abstract / Summary

Each year, the Tripoli Rocket Association hosts its Argonia Cup competition south of Argonia, Kansas for international collegiate and high school teams to put their rocket and payload designs to the test. The University of Colorado Denver Polaris Rocketry team is a continuation of the MACH Rocketry team and will compete in this years' competition. The Polaris Rocketry intends to place first in the competition which occurs, March 2021 and win the Argonia Cup trophy.

The team will be optimizing fin, airframe, nosecone, electronics bay, and payload delivery designs. The goal of these designs will be to achieve a minimum altitude of 8,000 feet above ground level (AGL) and to place a golf ball payload closest to a pre-positioned rendezvous point. The Polaris team will examine multiple fin, nosecone, and motor designs based on their performance, fiscal implications, and difficulty in manufacturing in order to determine an optimal choice for victory in the competition. The team has completed the initial design phase fluid analysis of the aerodynamics impacted components and hopes to begin to move to the manufacturing phase by the start of November 2020.

Table of Contents

List of Figures

5

Introduction

On March 27-28, 2021, the Polaris Rocketry team will be competing in the annual 2021 Argonia Cup. The goal for the competition is to launch a rocket powered vehicle containing a golf ball payload to a minimum altitude of 8,000 ft AGL and to recover the payload safely at a predetermined location on the rocket range. In order to maintain fairness and safety the competition has posted a list of ten rules. In addition to the list of rules launch operations guidelines, scoring and even a video submission required to compete in the competition.

The rules for the competition include;

A. Having at least one Tripoli Rocketry Association (TRA) certified Level 2 member per team. This member must be present for the entire duration of the competition and all other team members must be currently enrolled at the competing college.

B. The maximum installed impulse for this competition will be a commercially available 5,120 Newton Second motor. Motor clusters, air starts, multi-stage motors, and spark-emitting motors configurations are prohibited.

C. Any deployable payload shall limit the descent velocity to less than 30 feet per second.

D. Any propulsion/steering system designed to recover the payload cannot be used to boost the payload to the target apogee.

E. A commercially available, altitude recording altimeter with onboard data storage will be used for altitude determination and may be used for payload deployment and/or rocket recovery. If two or more altimeters are used, the averaged apogee height of each altimeter will be used for determination of rocket apogee.

F. Launch vehicles shall be launched at an elevation angle between 83 and 85 degrees (5 to 7 degrees off vertical). All flights will be angled away from the flight line regardless of wind direction.

G. All flights must have a minimum of a 5:1 thrust to weight ratio at liftoff.

H. Launch configuration flight stability shall be achieved by maintaining a minimum CP/CG static margin of no less than 1 body caliber during flight.

I. Apogee must occur at or above 8000' AGL (field elevation is approximately 1249' MSL). Any flight not reaching this altitude will be disqualified and each team may make up to three flight attempts with the closest qualified landing score being their official flight.

J. The rocket's launch vehicle components will be recovered in a condition that allows it to be flown again after the first flight.

On the day of the competition, there will be certain launch operations followed directed by the Tripoli Rocket Association (TRA):

K. The launch organizers will provide all launch pads, launch rails, and the launch control system. Both 1.5" x 1.5" (commonly known as 1515) and 1" x 1" (commonly known as 1010) rails will be available in 12' lengths. A minimum of two (2) rail guides must be used.

L. All rockets will be subjected to a rocket safety inspection before the teams will be cleared to fly their projects. Any safety of flight issues noted in this inspection will be resolved before flight. These safety inspectors have the final say regarding any project's suitability for flight.

A winner for the competition will be determined by scoring guidelines. Prior to the start of any launch activities, the location of the landing target will be clearly marked and will be available for inspection by the competing teams. The landing target will be established by the launch organizers and will be within line-of-site and not more than 300' from any launch pad location. At the completion of each flight, the distance from the center of the payload to the center of the target will be measured by the launch organizers before the teams are allowed to remove their payloads. The point of initial touchdown will be used if it can be determined in the event of the payload skipping across the surface. The rocket team who lands the golf ball payload closest to the designated landing spot will be declared the winner, unless multiple teams tie in the distance. In that case, the team with the highest altitude for apogee will be declared a winner.

Main Airframe and Overview

Design

The airframe consists of a cylindrical shell, with breaks above the engine and above the electronics bay, providing ejection space for the recovery system (drogue and main parachutes) to be deployed. The airframe is the main structural member of the rocket and must display enough resiliency and structural integrity to achieve a stable flight. The overall dimensions of the airframe were chosen in the initial design stage, and were based, in part, on the size of the L-1000W-18A motor as well as the payload constraint considerations. The L-1000W-18A has an outside diameter of 54mm (2.125") and an overall length of 635mm (25"). The payload is expected to have a nominal diameter of at least 3.5". Therefore, a 4" diameter was selected as the nominal ID for the airframe. Owing in part to the availability of materials that could be used for mandrel fabrication, as well as providing ample space for the payload to easily fit into the payload section of the

9

airframe, the final design was decided upon. To provide ample room for design and manufacturing adjustments, initial mandrel length was selected to be 5'. The final length of the airframe sections was decided as a result of the electronics bay and drone designs as they evolved. Based on these parameters, Body Section 1, defined as the lower section of the rocket, is 30" long. This will provide ample space for the motor and for the drogue parachute to sit in. Body Section 2, defined as the second (middle) section of the rocket, is slated to be 36" long. This will provide space for the electronics pay, payload, and main parachute.

Analysis

In order to gauge the efficacy of using a carbon fiber wind for the airframe and motor mount sections, compressive testing was warranted. In order to test the airframe before it was built, to limit the amount of time lost, an airframe from a previous semester was tested. Given the information that the previous team passed on it was determined that the new airframe would be stronger. Thus, the new 4" airframe section could be verified by the data from previous semesters with the assumption that the old airframe would be of worse quality. The old airframe was also constructed using the X-Winder, although it used a lower angle for the lay pattern. Giving it a similar base structure, though one that would not be quite as strong as ours.

In order to achieve the most accurate results an ASTM testing standard was referenced. Upon examination of this testing procedure, it was noted that the length of rocket airframes tested is usually 2-calibers with reference to the diameter of the segment being tested. As the previous rocket was 6-inches in diameter, 12-inch sections were cut to conduct the test. Two sections would eventually be cut, one which was the top of the airframe section that included much more filament

due to operating errors. This section was designated Airframe Section 7104. The second tested airframe section was also 12-inches long and was immediately beneath the previously mentioned section. This airframe section was designated Section 7107. Both airframe sections were thoroughly sanded down with 400 grit sandpaper in order to present the Instron machine with as flat and even a surface as possible.

Measurements of both airframe pieces were taken with regard to their inner diameters, outer diameters, and total length, these dimensions can be seen in Appendixes F and G. Both samples were taken to the North Classroom lab to use the Instron machine, which can apply up to a 120-kip load. The breadth of the Instron machine is 6.25" in, meaning that for the 6" airframe pieces did not have sufficient clearance to minimize risk. The high tolerance could result in some slippage due to insufficient testing area.

Figure 1 - Airframe Section 7104 in Compressive Test

The compressive test was able to record the net displacement in [mm] of the airframe and a force in [kN] to which the rocket was subjected to. In order to find the airframe's strain, the displacement data was divided by the length of the rocket which was previously calculated. The stress was calculated by dividing the force that was applied to the airframe sections by the top surface area of the carbon fiber, which was found by subtracting the circular area calculated by the outsider diameter by the area calculated from the inner diameter. When plotting the section's pressure against its strain, the material's elastic modulus was found by calculating the slope of the primary line until failure.

Section 7104 was able to achieve a maximum compressive force of 38.670 kN before it experienced a failure. Failure occurred when the airframe was displaced by 13.631 mm. Based on the slope of the graph displayed, an elastic modulus of 14.9856 GPa was calculated. Section 7107 was able to achieve an equivalent maximum compressive strength of 38.670 kN before it failed, However, this occurred when a mere 3.0696 mm of airframe was displaced. The calculated elastic modulus based on the graph displayed was 10.947 GPa. This is 26.95% less than that of Section 7104. This was expected due to the higher resin makeup of section 7107.

At first glance, the strength of the *RocketLynx* airframe appears lower than expected, however several considerations must be made. The tested airframe was not wound with the ideal techniques that would result in the highest possible compressive strength. Due to failures in the G-code utilized, the layers for the tested airframe were made with haste and were not evenly distributed. This led to several sections where extra resin and fibers were stacked. The unevenness in the fiber lay thus leads to micro-buckling and earlier part failure. In addition, the ideal low-winding angles

of approximately 30° was not used. Most of the airframe section angles were approximately 70° from the horizontal, creating a weaker structure. The *Polaris* airframe will feature winding angles that are much closer to 30° than the *RocketLynx* airframe. Based on these aforementioned factors it is assumed that the Polaris wind schedule will result in a much higher elastic modulus. The previously conducted *OpenRocket* simulations have indicated that the *Polaris* rocket will also undergo much smaller stresses for shorter periods of time than the previous rocket. As a result, it can be assumed that when combined with superior winding procedures, similar average wind-thicknesses, and lower experience stresses, that this year's rocket will be sufficiently structurally sound.

It is important to note however, that a limitation of this test is that each wind will be different. Although these tests give the team a rough idea of carbon fiber's capabilities, an ideal test would include an actual section of a motor mount or airframe that was wound by the team. This test would yield exact results for our fiber lay and resin content.

Materials Selection

The primary goal in choosing an airframe material is choosing one that will accomplish three main tasks. That is; the material must have a high elastic modulus, the material must be as light weight as possible, and the material must be thermally stable. Analysis of the materials readily available to the team yielded two options: fiberglass and carbon fiber. Both of these materials are meet the three aforementioned criterial and are relatively cheap to produce and manufacture. However, of the two materials, carbon fiber is much cheaper. The only side effect that this has on our mission is that carbon fiber is not radio transparent and acts as a faraday cage. Because our GPS will be

13

housed out of the nosecone of our rocket this is not a concern. Thus, based on these criteria and considerations, wound carbon fiber is the best candidate. Taking the advice of composites expert Kevin Fornell, we then selected a resin mixture and fiber type. Since other groups have historically used this material as well, we were able to acquire what we needed from the shop's supply depot.

Manufacturing

The information obtained during the first stages of our composite-design and manufacturing trials have guided us forward with some valuable lessons and insights about how to achieve a more successful filament wind. Initially, the plan was to proceed with a winding schedule for the 4" airframe tool using a 3-axis wind without end caps. This was in anticipation of the first collapsible mandrel design, shown below in Figure 2.
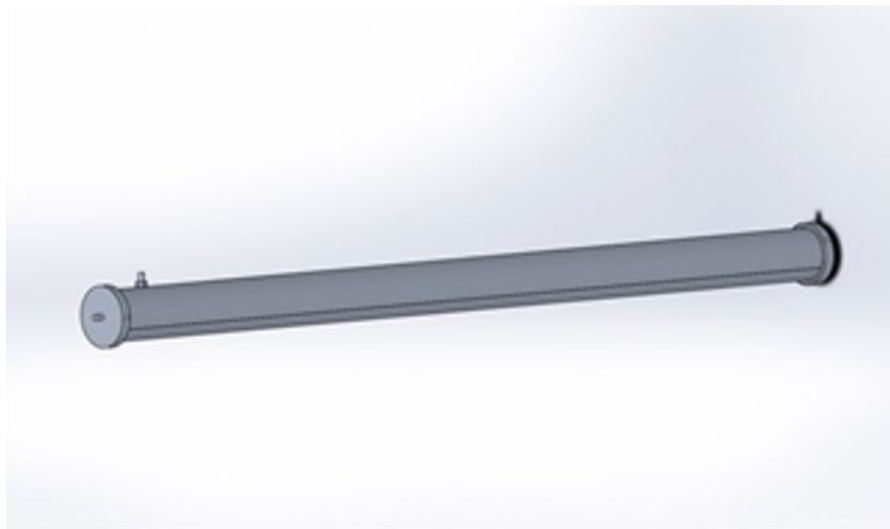
Figure 2 - Original Mandrel Design

Based on test dry winds and the motor mount wet wind, it was found that this method would be unsuitable for 3-axis winds as was initially hoped. The winding angles in the dry winds were rather

14

limited when using this method as the tension for the filament would have prohibited any angles greater than 45° from the horizontal to be used. This was because the wet filament had the tendency to slip as the carriage changes direction. This problem was encountered by a previous *RocketLynx* team when they were constructing their 6" diameter airframe several years ago. In addition, another issue experienced was the disproportionate amount of filament build-up at the ends of the carriage travel. The additional filament is the result of additional end wraps the program inserts in an attempt to hold the filament in its place. In theory, the technique would work, however in practice the excessive build-up results in the filament sliding off of the high regions, resulting in a misalignment. This can be seen in Figure 3.
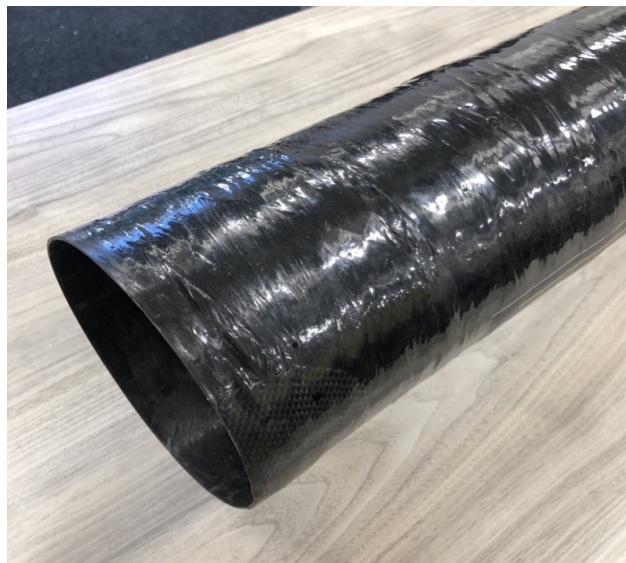
Figure 3 - Previous Team's Airframe

It was *Polaris Rocketry's* hope to overcome these limitations with the X-winder and to achieve a proper alignment of the filament within the airframe and motor mount constructed this year. In turn yielding a considerably stronger composite structure. As a result, it was decided that a longitudinal end wrap winding schedule, which can only be achieved through 4-axis winding with

15

hemispherical ends would have to be done. To accomplish this, a new mandrel was designed with disposable hemispherical end caps that would hold the panels in the correct shape.

The mandrel is completely collapsible and held together only by the filament itself. The proposed winding plan is to assemble the panels around the two-piece spacer discs and mount them onto the two end caps. Once in this configuration, 4" custom clamps are used to secure the piece as a whole. At this point, the clamped mandrel will be mounted onto the X-Winder and an initial hoop winding schedule will be used to fasten the panels together. Since the X-Winder is capable of pausing during a program, this will allow for the removal of each clamp as the 90-degree hoop winds approach. Once the middle section is fully hoop-wound, the mandrel will then be ready for longitudinal end-winding to commence. The mandrel, endcap, and spacer disc configuration can be seen in Figures 4 and 5.

Figure 4 - Proposed Mandrel Design (Closed)
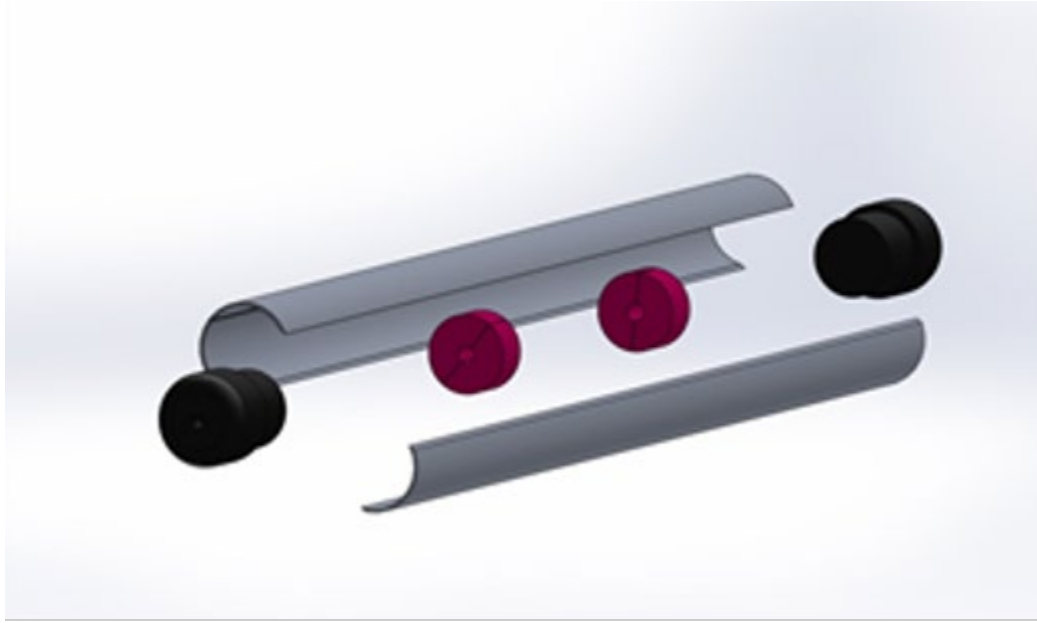
Figure 5 - Proposed Mandrel Design (Open)

This tool will function in a similar fashion to the previous tool used in the motor mount fabrication in that the ends are both to be sawed off and disposed, leaving the desired cylindrical section of composite structure behind. In the following figures, the manufacturing process for the mandrel panels is shown. The end result of milling the separate tubing sections into the appropriate sizes was good. The panels were all milled within a tolerance of 0.010" and fit together with minimal post-processing (deburring, filing).

Figure 6 - (Left) - Milling the bottom ⅔ section of 4" mandrel

Figure 7 (Right) - Resulting 'dry' assembly of mandrel panels

One main challenge with this design has been how to handle the 'ends' where the filament is being wrapped around hemispherical end-caps. With this design, there is no hardware of any sort that attaches the panels to the bulkheads or to the ends. To handle these problems, two solutions were first proposed: (1) attach the panels together around the assembly with two layers of paper and packaging tape, with the plan for the friction of this assembly being enough to drive it on the X-Winder, and (2) to install one hemispherical piece on each end to serve as a disposable mold to be sawed off and discarded after the initial curing was complete. The cost of having fully discardable end caps manufactured through conventional machining of engineering plastic was prohibitive. At 4" diameter and 6" of needed stock length, the cost per set of acetal (Delrin) end-caps was going to be \$75/wind. Thus, the design was changed, and the single-piece end cap was split into two pieces, with a reusable inner piece made from the Delrin round stock, and a hemispherical end cap that is disposable. Below is a figure showing the current prototype design, which will be further optimized for cost.

Figure 8 - Current Endcap Prototype Design

Thus, given the parameters aforementioned, a combination of different design proposals was constructed. The main portion of the mandrel was covered in a mold release agent (Zyvex) and a combination receipt paper/packaging tape to allow the mandrel to be easily removed. The ends of the mandrel were constructed out of a combination of foam and Delrin. Delrin stock was turned down so that it would fit inside the main airframe section and drilled and tapped for a threaded rod. Following the Delrin was a section of foam which was turned into a hemisphere with a flat end and threaded insert. This hemisphere attached to the Delrin through the threads and provided a mounting point for the travel carriage to attach. Figure 9 below is a representation of the final mandrel attached to the X-Winder carriage.

Figure 9 - Body Mandrel on Carriage

After an initial test of the program and initial wet wind a problem arose with the aluminum portion of the mandrel slipping against the Delrin portion. This resulted in problematic misalignment of the filament during winding. In order to resolve this issue a Delrin plug was cut so that the mandrel and Delrin had a point to grab and pivot upon. This plug allowed the stepper motor to drive the tool without any slippage, while also allowing the plug to still be pulled straight out from the finished part. Figure 10 below is the final fixture for this part.
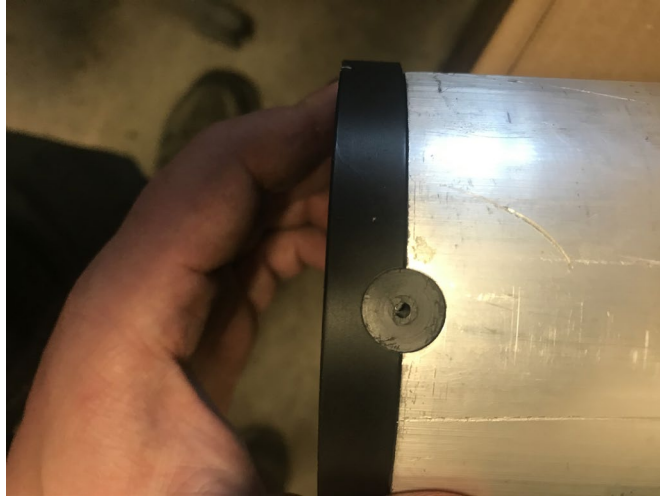
Figure 10 - Catch Plug for Body Mandrel

During the wind for the main airframe sections, it was noticed that the foam end caps tended to slip during the initial layer of the tow application. One cause of this issue was that the clearance hole of the foam tended to be too tight and allowed no clearance between the center of the cap and the all thread rod holding everything onto the machine. The first fix for this issue was to widen the clearance hole to allow for the 'bend' in the all thread support rod. Secondly, regarding the slippage of the hemispherical cap, in order to fix this a proposed solution similar to that of the Delrin and aluminum is proposed. In this solution the foam would have a protruding portion that inserts into the Delrin to prevent slipping. Although this would have helped to improve the initial layer slightly the overall performance of the mandrel was not impacted and thus the design was not adjusted for the second airframe wind. This will result in a cohesive and boundaryless transition between the upper and lower airframe sections.

For all of the minor issues that arose during the winding and usage of the collapsible tool, it worked remarkably well! The resulting part took about an hour to remove from the tool. First, the

hemispherical ends were band-sawed off (30 minutes). Next, the half-plugs are removed. Finally, the panels are pried out into the inside of the finished part, with minimal effort to do so.

The final part was measured to have a inside diameter measuring 4.020" ± 0.030". Considering the thin-walled tubing having a tolerance of ± 0.015" We were quite pleased with the finished result of the part geometry. The figure below is the mandrel and body tube after the first wind and shown disassembled for re-use.

Figure 11 - First Body Tube After Removal from Mandrel

Post-treating/Oven cure

Part of the process of creating strong structural members for the airframe includes heat curing the entire mandrel. This is evident as after the airframe was cured at room temperature the structure was very weak and could be cracked if the tube was compressed along its diameter. According to manufacturer specifications the heat cure cycle for the resin and hardener that was used should be

22

176F for at least 15 hrs. According to composites expert Kevin Fornell this is more time than is necessary and at a higher temperature. According to his expertise a 10 hr cure at 150F will be more than enough to re-bond the resin to the tow and increase our strength by at least 40%. Given the time constraints of the competition and the relative strength increase that the parts will already experience, the lower temperature and shorter time was deemed sufficient for the purposes of this launch. In order to maximize efficiency of the parts to be cured the full assembly was made before the curing process was completed. This assembly includes the motor bulkhead, fins, motor tube, centering rings, and body tube. The centering rings are glued into both the motor tube and the lower airframe section. The fins are slotted through the lower airframe section and glued to the motor tube and airframe section respectively. A picture of this assembly can be seen in the figure below.

Figure 12 - Assembled Lower Airframe Section

In addition to the lower airframe assembly the upper airframe section and couplers were also heat treated. All three of these components were able to fit into the heat cure setup such that only one cure cycle would be needed. The tangent ogive shape of the nose cone proved to be sufficiently strong such that it did not need to be cured. Additionally, a nylon fixture had already been installed for the aluminum tip to attach. The risk of having CTE issues or part failure due to the extra component was too great to justify curing the nose cone with the other parts. After the cure cycle was completed, there were no issues getting the parts to fit back together and a significant increase in structural soundness was observed.

Nose Cone section

Carbon Fiber Section

Design

The high-power rocket nose cone design is primarily decided on the basis of three main parameters; its drag coefficient, the maximum altitude achieved by the nose cone, and its weight. *Polaris Rocketry* has examined over fifteen nose cone variants with these parameters in mind. The goal of which was to determine the best design for the rocket's nose cone section and to determine their drag coefficients, including wave drag, frictional drag, and base drag.

The first design consideration, nose cone length-to-diameter ratio, was adjusted for maximum efficiency. Multiple shapes within each length-to-diameter ratio category were also examined, such as a conical shape, and multiple different ogive shapes each with different enclosure angles. Each nose cone was put through a Solidworks fluid simulation to examine what forces,

temperatures, and stresses that a nose cone with those shape parameters would undergo during launch and flight. Drag coefficients were calculated based on the simulations' data.

The final primary consideration includes the choice of design material, which requires an analysis of the design shear-stresses and the wall temperature experienced and is further analyzed under the material selection section.

The drag coefficient calculations for each nose cone were based on the forces exerted on each cone F_D , in Newtons. F_D was calculated based on the Solidworks simulation data. Moreover, the air density at altitude, ρ, was found based on an *OpenRocket* simulation which predicted a maximum vertical velocity of 515 m/s. This velocity was achieved at approximately 1,768 m above sea level, where the density of the air is $1.031 \frac{kg}{m_3}$. The frontal cross-sectional area, A, was calculated to be $0.008107 \ m^2$. Equation 1 was used to calculate the final drag coefficient given the forces found in the fluid simulations.

$$C_D = 2 \ F_D / \rho V^2 A \qquad \qquad Equation \ 1$$

In addition to the Solidworks' drag calculations, hand calculations were done to obtain a second set of drag coefficients. These calculations were done as a quality assurance method to verify the results obtained in Solidworks. For the hand calculations, the total drag coefficient for each nosecone includes the sum of the frictional drag, C_D, F, base drag, C_D, B, and wave drag, $C_D, \ W$. The total drag is shown in Equation 2:

25

$$\left(C_{D_0}\right)_{Body} = \left(C_{D_0}\right)_{Body,Friction} + \left(C_{D_0}\right)_{Base} + \left(C_{D_0}\right)_{Body,Wave} \qquad Equation\ 2$$

The equation to find the frictional drag is displayed below as Equation 3. Where the frictional drag from a sharp nose cone can be found through the length-to-diameter ratio of the nose cone in calibers, l/d, the Mach number M, and the dynamic viscosity, μ, of the air at the altitude at which the Mach number is attained q, and the length of the rocket, l.

$$\left(C_{D_0}\right)_{Body,Friction} = 0.053 \left(\frac{l}{d}\right)\left[\frac{M}{ql}\right]^{0.2} \qquad Equation\ 3$$

The base drag is found by multiplying the square of the Mach number the rocket attains by 0.13 and adding it by 0.12, as shown in Equation 4 below:

$$(C_D)_{Base} = 0.12 + 0.13\ M^2 \qquad Equation\ 4$$

Wave drag, which is induced upon any sharp nose cone can be found using the variables of the Mach number, M, and the length-to-diameter ratio of the nose cone design, l/d. It can be seen in Equation 5 below:

$$\left(C_{D_0}\right)_{Body,Wave} = \left(1.586 + \frac{1.834}{M^2}\right)\{tan^{-1}[0.5/(l_N/d)]\}^{1.69} \qquad Equation\ 5$$

Of the fifteen designs, nose cone lengths of 1.5-, 2-, 2.5-, 3-, 5-, and 5.5-calibers (L/d) in length were examined to find the force patterns, overall drag coefficients, and wave drag. Generally, it is stated that nosecones with a larger caliber sustain lower drag forces, than nose cons with smaller calibers.

Analysis

1. Drag

Research and analysis of nose cone design shows that, in general, for any design where length-to-diameter ratios is held constant, conical vs ogive shape makes little difference in the expected speeds attained. For tested values, the final velocities, when only changing shape parameter, range from Mach 1.23 to Mach 1.16 for a 2-caliber long ogive design and a 2-caliber long conical design respectively. Additionally, all ogive nose cones tested were able to bring the rocket up to at least 8,100 ft or higher in altitude with the L1000W-18A motor, while the conical nosecones were only able to achieve the minimum altitude of 8,000 ft when the length-to-diameter ratio was at least 3-calibers. The drag coefficients for both conical and ogive designs decreased as the length-to-diameter ratio increased. Both designs started with drag coefficients of around 0.59 for a 2-caliber nose cone. An increase to 2.5-calibers dropped the drag coefficient to between 0.50 and 0.52 and additional 0.46 or 0.47 for a 3-caliber length. When tested at 5 and 5.5-calibers, the rate of decrease in drag coefficient was less significant, with both staying within a range of 0.38-0.42 range. The results for the conical nose cone drag coefficients can be seen in Appendix A.

After examining the low drag coefficients of the 5- and 5.5-caliber nose cone designs, an ogive or conical design had to be chosen for each caliber. According to equations 3 through 5, a 5-caliber ogive nose cone would provide, of the four designs, the lowest drag coefficient, while achieving the largest altitude AGL of 9,020 ft given our current rocket layout. This is in contrast to 8,390 ft for the same caliber conical nose cone. The flight simulations for conical and ogive nose cones can be seen in Appendix D and Appendix E respectively. Given this information, a determination was made that the 5.5-caliber conical and ogive designs did not offer a low enough drag coefficient to

27

compensate for the increased weight compared to the shorter 5-caliber design. As a result, a 5-caliber design, in both the conical and ogive shapes, was preferred. Both the ogive and conical nosecones had similar drag coefficients for their respective length/diameter-ratios, with the ogive nose cones generally being slightly lower than that of their conical counterparts. As a result, the 5-caliber ogive nose cone was chosen as the final design. The results for the conical nose cone drag coefficients can be seen in Appendix B.

Hand-calculations confirmed all of the results found with the Solidworks simulations. When compared, both numbers are remarkably similar given the complexity of the problem. The difference between the averages of the hand-written and Solidworks simulations is 3.33% and 15.63% for the conical and ogive nose cones respectively. As seen in Appendix C, the slopes from one l/d to another were nearly identical, showcasing the studies' repeatability. The only inconsistency of note was for the 2-caliber ogive simulation, which featured a 0.76133 drag coefficient with the Solidworks simulation compared to the 0.59456 coefficient found with the hand-calculated equations, a difference of 28.05%. However, based on the trajectories for both the Solidworks and hand-written results, it is likely that the computer simulation was inaccurate for the 2-caliber ogive design, and should be significantly lower than what was projected. The drag coefficient results for the ogive design can be seen in Appendix B.

2. FEA

Stress testing was conducted on the nose cone and body sections, for which a force was applied parallel to the wind direction. The force applied was calculated using the fluid simulations that were previously conducted and aforementioned. Specifically, the force on the nose cone was

28

calculated using the Solidworks built-in force calculator for a given airspeed and vector direction and on a static body. This simulation determined that the maximum force on the nose cone would be 375 N. In order to maintain a safety factor of minimum 2, this finite element analysis was conducted with a vertical test force of 750 N. This test configuration would sufficiently provide results pertaining to the stresses and strains imparted on the rocket by the forward velocity of the launch and the potential of shock waves from breaking Mach Number 1. Finite Element Analysis (FEA) determined that the maximum von Mises stresses imparted were on the magnitude of 2.5 MPa. This was concluded using the finest mesh possible for this type of solid meshed FEA simulation. Specifically, the element size was 0.5" and each element was held to a 0.025" tolerance. The mesh consisted of a 16-point Jacobian High-quality mesh. It contains 57,649 nodes and 30,254 total elements. The majority of nodes had an aspect ratio between 3 and 10 at 91.67%. There were no distorted elements given these parameters. All applied forces were defined to be in a uniform distribution on the forwardmost face of the rocket. They were defined to be in the direction of flight, which is assumed to be stable. A single fixture, located at the aftmost surface of the aft body section, was created to maintain equilibrium along the length of the rocket and simulating a fully developed flight profile. No other fixtures were needed given the direction and parameters of the flight in this stage. Given these stress parameters, the maximum deformation can be observed through the figure below. This figure shows the deformation of the rocket body and nose cone on a 1,000x deformation scale. Meaning that the deformation visualized is 1000 times that of what it would be during flight.
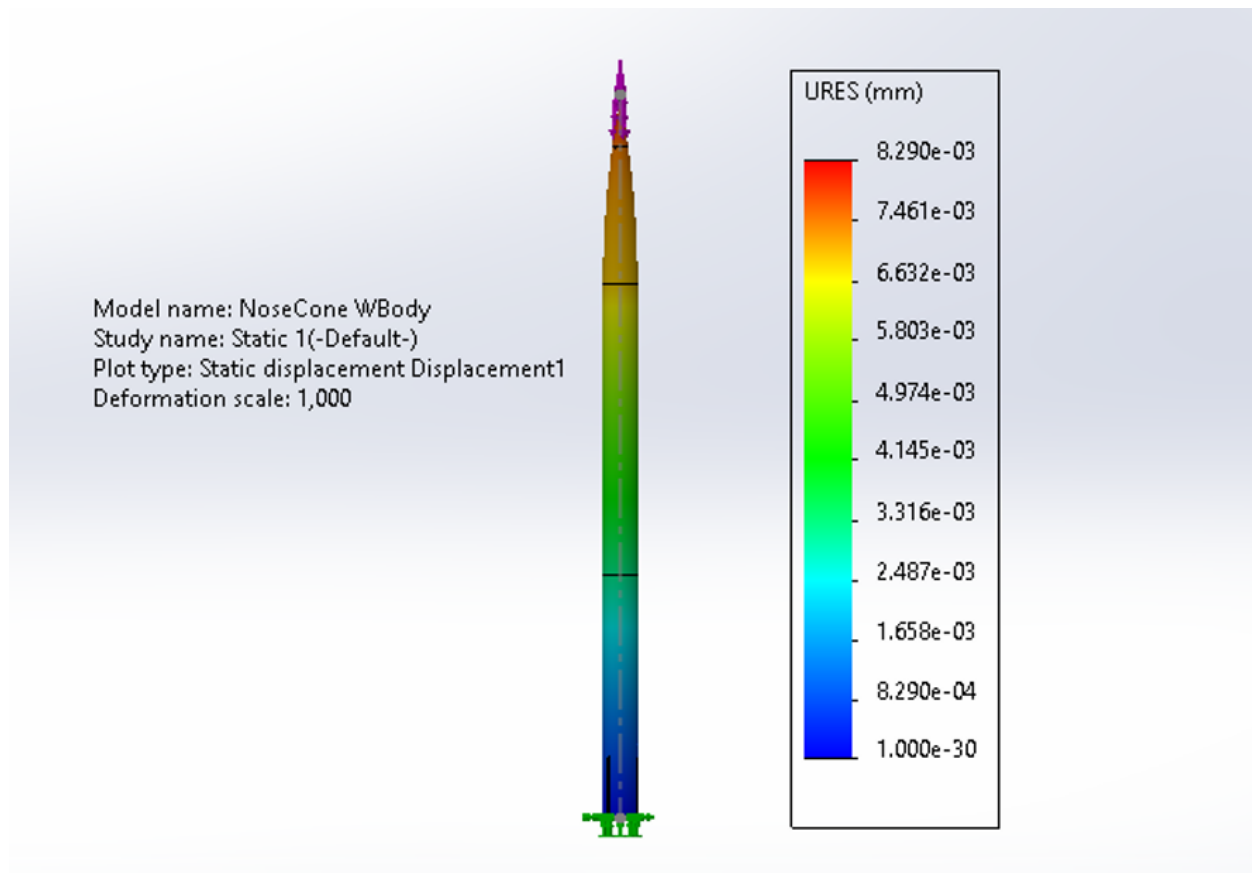
Figure 13 - Displacement Graph of Airframe Body

Upon further examination, it is observed that, although the deformation upon the length of the rocket appears to be of great magnitude at the foremost part of the rocket, which is the maximum value, a deformation of only $8.3 \; x \; 10^{-3} \; mm$ is observed. This is only $3.26 \; x \; 10^{-4} \; in$ which is less than the tolerance for all the parts used in our assembly. Based on this information it was concluded that the parts will not fail, even for a safety factor of 2 and that the rocket will successfully reach apogee given the force and material properties. A free body diagram can be seen in the figure below.
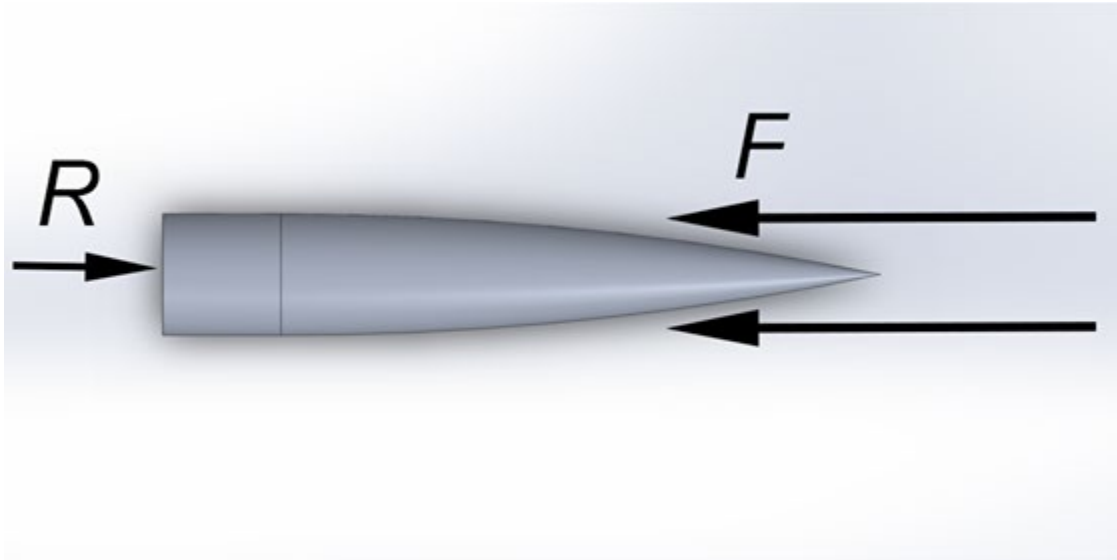
Figure 14 - Nose Cone FBD

Materials Selection

Two primary concerns were raised about the material selection, the first being the weight of the nose cone, which needed to provide at least one-caliber length in stability between the center of gravity and center of pressure. The second concern was determining a material that would be able to withstand the stresses and temperatures that come with supersonic flight. This became increasingly apparent as all simulations indicated that speed of approximately Mach 1 would be attained. After settling on a 5-caliber ogive design, fluid simulation tests predicted that the nose cone would experience a maximum of 571.94 Pa of shear stress with a total pressure of 408.02 kPa, and a maximum wall temperature of 415.13 Kelvin.

Based on each components' current projected locations in the rocket, a heavy nose cone would be needed to shift the center of gravity forward, leading to the requirement for a dense material to be selected. Thus, G10 fiberglass was selected due to its thermal, density, stress, and radio-transparent properties. Even considering a dense nose cone design further weight is needed. An aluminum tip

31

will be added to increase the forward lean of our weight distribution. G10 fiberglass has a tensile strength of 276.9 MPa, which is far higher than the shear stress and pressure requirements. Additionally, fiberglass has a somewhat high density of approximately 1.86 g/cm^3, which aids in shifting the center of gravity forward. This statement assumes a 0.25" wall thickness which is much thicker than needed. G10 fiberglass is also cited as having a continuous serviceable temperature in the air of 414 K. It is notable to mention that this is slightly lower than the 415 K temperature that the rocket will temporarily experience. Considering the rocket will only momentarily breach the sound barrier, it was decided that this was an acceptable risk to take. Lastly, fiberglass is radio-transparent, meaning that any potential electronics that may be placed in the nose cone in the future will be able to transmit radio frequency with limited interference.

Manufacturing

Manufacturing of the nose cone section of the airframe was a challenging and unique experience in regard to using the 4X-23 filament winder. The main challenge faced by our team in this endeavor was in creating a winding schedule that would achieve the tangent ogive profile of the nose cone design. The 4X-23 X-Winder itself is a four-axis machine tool, capable of executing complex maneuvers in four simultaneous degrees of motion. The problem with the part profile was not in the machine capabilities, but rather the software limitations of the design software that the X-Winder is powered by and how they related to the filament-winding process of creating a conical shaped part.

The designer software operates based on simple inputs that the user selects for the part profile. These include the part diameter on each end, the part length, the spindle RPM, as well as details regarding the polar ends of a 4th axis wind.
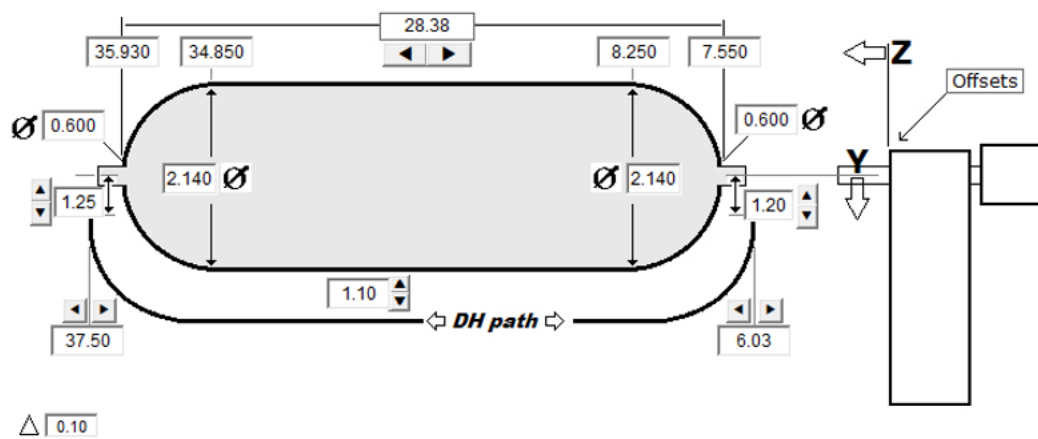
Figure 15 - Picture of Designer Software Inputs

The original design hoped to use a 4th axis toolpath in creating the nose cone, with the disposable end caps that we have used for winding of the main airframe and coupler sections. This however would result in uneven filament buildup corresponding to the ratio of the diameters from the big end compared to the small end...i.e. Having a 4" diameter on the left end tapering down to a 2" diameter on the right end would result in a 2:1 discrepancy in filament deposition. There was no way around this issue, as long as we were winding filament around polar ends, and thus the technique was quickly abandoned.

Alternatively, the possibility of achieving the wind with a 3-axis toolpath was explored, using a mold for a core and having disposable, cylindrical end caps on either end, and with no polar caps at all. This technique seemed possible if the g-code for the X-Winder could be manipulated to

33

allow for a higher fidelity tool path. The first attempt at this winding schedule was to simply use an average diameter of the part equal to

$$D_{ave} = \frac{(D_{min} + D_{max})}{2} = \frac{(2+4)}{2} = 3"$$ *Equation 6*

By simply inputting the nominal part diameter of the nose cone as 3 inches, and by selecting appropriate values for the other part parameters, a first attempt was made, with inadequate results.

Figure 16 - First, Unsuccessful Winding of Nose Cone

As is visible in the image, the filament after one 'complete' layer does not entirely cover the nose cone mandrel and has other problems as well. The buildup in the front in thicker, at 1.5 the nominal desired amount, and the filament in the rear is lacking, at 0.75 the amount that the designer software calculated for the average part diameter, D_{ave}. Additionally, the filament is not laying flat against the mandrel surface at the front of the nose cone, but rather is tilted up, with the leading edge slacked and the trailing edge taught against the mold. It may have been possible to simply wind

34

over these imperfections and achieve full coverage of the part, but the structure would not be intact, and would certainly fail during transonic and supersonic flight, where it would experience significant loading.

The g-code for the X-Winder is standard g-code language with a few machine-specific differences. For our purposes we planned on first manipulating the 'acceleration' values for the linear acceleration. This plan did not work however, and a new strategy was implemented. Below is a screenshot, courtesy of X-Winder, showing the basic g-code pieces and explaining their functions. Here, each axis is controlled using specific g-code parameters.

Movement Commands
G-Code Letter Designations

Position (in or mm)	X	Y	Z
Linear Rate (in/s or mm/s)	D	E	F
Linear Accel (% of Full)	I	J	K
Angle (deg)	A*	B	C
Angular Rate (RPM)	Q	R	S
Angular Accel (% of Full)	N	O	T

Note: (1) A can also designate cumulative Mandrel Rotation Angle
　　　　(2) Angle directions and rates follow right hand rule
M5 = Mandrel Stop

G2, G3, G4, G5, G6 are Coordinated Timing Movements
Action is considered complete when the slowest axis movement completes
Once all axis movements are complete, program begins to execute next line of g-code

Figure 17 - X-Winder G-Code Key

Post-treating/Oven cure

Examining the design of the nose cone and nylon threaded insert for the aluminum tip it was determined that the part did not need heat cured. The tangent ogive geometry of the nose cone provides significant support and reaction force against the head wind caused by the rocket

trajectory. Additionally, this shape provides significant transaxial support that prevents the part from compressing through its diameter. Unlike the brittle airframe sections and motor tube, if the nose cone is compressed it does not crack or buckle for a significant amount of force. During the process of fitting the aluminum tip to the carbon fiber nose cone a nylon fixture was added to create a mounting point for the two parts to merge. Due to the addition of this part concern was raised about the thermal expansion of the pieces and unforeseen consequences during the cure process. Considering the summation of all these factors it was determined that the nose cone did not need to be cured further and would sufficiently achieve its goals.

Aluminum Tip

One of the fundamental functions of a nose cone is to break the airstream which leads the rocket body and to reduce the aerodynamic drag. The process of breaking up the airstream and reducing the drag has secondary effects on the surfaces performing these tasks. In addition to the forces applied, a significant amount of heat is introduced to the leading member. Thus, the greater the velocity of the airframe the greater the increase in heat. Additionally, the center of gravity of the rocket needs to be as far forward as possible. This will ensure the greatest possible stability caliber given our configuration. Adding an aluminum tip to our rocket will help to solve both of these problems. The added weight of the metal will push the center of gravity forward and the aluminum will serve as an excellent heat sink.

Design

The aluminum tip will be the leading member of our rocket and will experience the brunt of the forces due to the drag and heat transfer. Based on Open Rocket simulations and the known weights

of each piece our rocket is estimated to have a caliber of 1.75 with a 6" aluminum tip. This puts us exactly in the middle of our acceptable range concerning caliber (1.5-2). In order to connect to the carbon fiber portion of the airframe the nose cone is threaded on the flat end. This provides an anchor point for the threads to attach firmly and provide sufficient holding force to prevent separation. The weight of the aluminum tip after these features have been added is approximately 16 oz and the length is 6". The end of the component was rounded for safety with an ⅛" end mill.

Materials Selection

Given the nature of what the tip of the nose cone needed to do aluminum was the most logical and practical material. Aluminum provides sufficient weight such that the center of gravity will be moved far enough forward without compromising the total weight of the rocket and is sufficiently thermally conductive so that it can withstand the temperatures of going to Mach number 1 and staying in the transonic region.

Manufacturing

The aluminum tip was made from 6061-t6 aluminum bar stock and turned down on the CNC lathe. The process design was to have the interior of the tip complete before turning the tangent ogive profile commenced, to simplify fixturing and to eliminate the need for any special soft jaws. After the back side of the tip was drilled and tapped to the design requirements, the part was flipped around and the final profile was turned onto the part. . A program was written to cut steps into the stock roughing out the shape for the nose cone. Once the steps were cut finishing passes were made to smooth the part down to its final shape and dimensions. At this point, the tip was complete and

37

the final step was to use the 0.120" part-off blade to cut the tip to it's design length, and carefully catch it in a bucket.

Couplers

The purpose of a coupler is to hold together airframe sections during the launch and pre-ejection flight. Each coupler needs to be slip fit into the two sections which it touches. This ensures that when the ejection charges are set off that the airframe sections separate and do not get stuck to one another. Because the sections are slip fit to one another and not friction fit shear pins are used to keep the airframe sections together when the engine cuts and the rocket loses acceleration due to gravity.

Design

Because the couplers are intended to be kept within the airframes and nosecone, their dimensions are inherently smaller than that of the components they are kept in. The airframe's inner diameter stood at 4.020", so a coupler size of 4.010" was created with a 3.920 x 8.0" diameter mandrel. This required the section to be sanded down in order to comfortably fit within both pieces. The resulting fit between the couplers and the body sections are very firm yet allow each member to move against the others. The tolerances held by the X-Winder are not tight meaning that each coupler was sanded and turned so that they would fit into only one of the body sections or the nose cone.

Two couplers had to be created, one that would join the forward airframe and nose cone and one that would join the bottom and forward airframe sections. The former coupler would be eight inches long in order to provide a one-caliber length for the lower airframe section while providing

two-inches for the upper airframe section that it will be glued to. For the latter design, a six-inch overall length is needed to fit into the forward airframe. Four-inches for the upper airframe section and with the tapered-down nose cone only a two-inch section is needed.

The coupler that connects both the lower and upper airframe sections is intended to be epoxied on to the upper portion of the lower airframe. This will allow the electronics bay to be easily inserted into the upper airframe section and to be removed if necessary before and or after flight. The coupler that connects the upper airframe to the nose cone will be glued to the lower part of the nose cone, which allows for the easy ejection of the rocket's payload section and main parachute.

Analysis

The number of #2-56shear pins needed was placed at four, which is a standard number required for a 4" diameter rocket. The rocket simulation recommended four shear pins based on the 2.5 [g] black powder charge that was expected, let alone the additional 5.0 [g] charge that will be attached to the EasyMini for an emergency blowout.

Materials Selection

In the same vein as the airframe and nose cone, carbon fiber was chosen for the coupler sections because it was readily available. In addition, carbon fiber is renowned for being a strong and lightweight material, which is ideally suited for this application. The radio transparency of the couplers did not need to be considered since no electronics will be passing through the couplers.

Manufacturing

Following the design requirements of the couplers, the size for the coupler mandrel was selected in anticipation of the typical thickness of the carbon fiber, using four layers at approximately 0.060" for the layers and resin together. The nominal size of the main airframe tube ID was measured to be 4.020" and the coupler was designed to have a minimum wall thickness of 0.050". Thus, the coupler mandrel was turned to 3.920" x 8" in length. The fabrication of the coupler pieces was challenging in that their shortened length did not lend itself very well to the polar winding schedule that we had used previously on the main airframe sections. This was because the filament misaligned and lost tension at each end as it traversed the poles and resulted in a failed winding. For this reason, we selected a new winding schedule, using the machine's three-axis mode for the winding schedule. One challenge with this winding schedule is that the extra hoops at either end of the wind resulted in excessive filament build-up which then resulted in misalignment of the filament as it 'fell' from the thickened locations on the part. To try and overcome this phenomenon, we added reduced diameter Styrofoam sections at either end of the tool, where the built-up filament could have a place to evenly build up in diameter to a similar diameter as the design of the part. This is shown in the following figure.
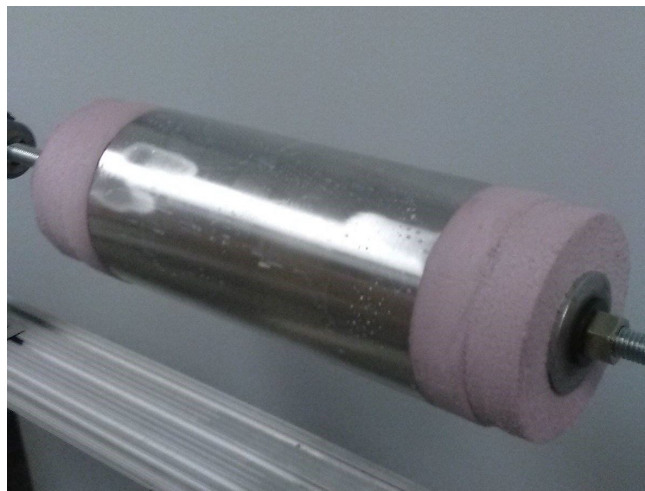

Figure 18 - Coupler Mandrel with Disposable Square End Caps Exposed

This technique worked reasonably well for the first several layers but did end up resulting in filament slipping as the layers stacked up. One recommendation that we will address further in our recommendations and path forward section deals with these 'disposable ends' for the three-axis winding schedule, and how to create a more successful winding schedule.

Sanding down the couplers was done with a mostly manual method using a CNC lathe to hold the couplers mandrel in place while the manufactured coupler itself was friction-fit onto the mandrel. The lathe was turned at 150 rpm while a Polaris team member would hold a piece of 240-grit sandpaper that was moved from left-to-right to slowly trim down the diameter of the coupler. After several hours, each coupler section was test-fitted into their pre-assigned section. If it was too large, the coupler piece was once again sanded on the lathe until it could fit in its entirety.

Bulkheads

Design

The bulkheads' primary purpose is to provide an anchor point for parachutes and to prevent components from moving once they have been placed in their final configuration. Each coupler was measured so that it fit inside the appropriate airframe section where it was needed. To provide clearance for the bulkheads to be inserted into the body of the rocket an outer diameter of 4.0" was manufactured. The airframe has an inner diameter of 4.02" in diameter leaving a 0.01" clearance between the bulkhead and rocket body. Each bulkhead consists of 0.25" thick fiberglass in order to provide for a high factor of safety. When strength testing was conducted our factor of safety was more than 3 with an uncured epoxy and fiberglass setup. In addition, the bulkhead sections

for the electronics bay would be holding the main and drogue parachutes, so a ½" hole was cut in the center to provide room for a threaded eye bolt. This will provide a mounting point for the parachutes. In addition, the bulkheads attached to the electronic bay have wire pass-throughs so that the ejection charges can attach to the EasyMini and TeleMega.

Analysis

Compression testing was done on a sample bulkhead piece that was made out of the same fiberglass that was intended to be used within the rocket. A sample piece from the second airframe mandrel was cut with a bandsaw in order to provide the housing for the bulkhead. Proline-4500Q resin and hardener were mixed together at the appropriate ratios, 100:16, and applied to the fixture to hold the bulkhead in place. The bulkhead was centered in the airframe test section and fixtured at a 90 degree angle relative to the airframe walls. A slight layer of the proline-resin mixture was lined around the edges of the bulkhead to form a bevel around the perimeter of the fixture where the bulkhead interacts with the airframe. This process was repeated on both sides creating multiple supporting elements for the bulkhead fixture. The resin was left to dry for 24 hours before compression testing began to allow the resin to fully cure and provide the best strength characteristics possible. A 2.125" diameter aluminum cylinder was cut and used to represent the motor which would be striking the bulkhead during the compression test. This cylinder was mounted to the Instron such that the forces applied would pass directly through its z-axis.

In order to best understand the bulkhead section, it was tested until failure. This allowed examination of the amount of force the bulkhead could withstand and a minimum baseline by which the factor of safety could be measured. It was also important to note whether the bulkhead

or body tube would crack before the proline-resin mix had failed due to the pressures put upon the center of the circle imparted by the motor. The machine was set to compress at 0.5 mm/minute with a gradual increase in force. The results are as follows:
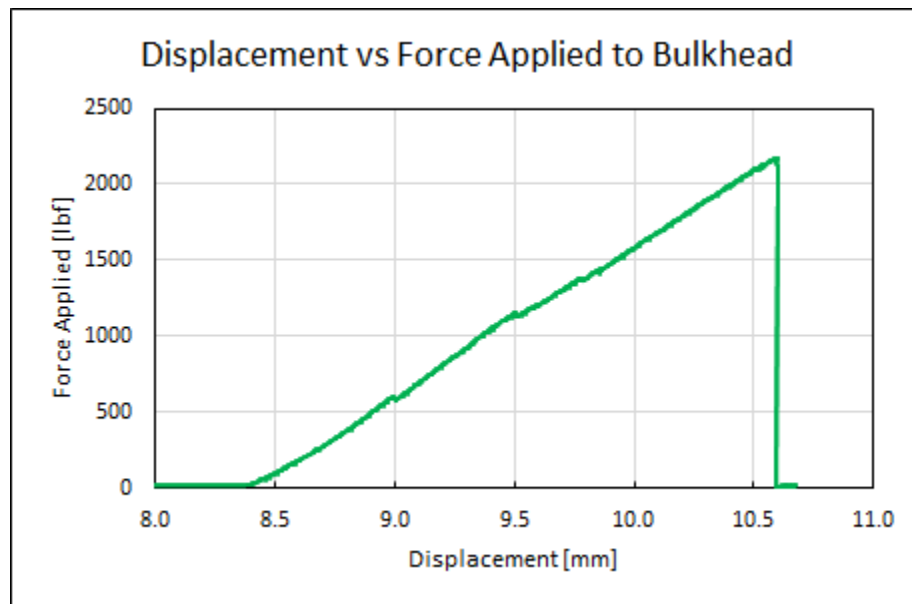
Figure 19 - The Quantitative Results of Compression Testing the Bulkhead Section

The compression test highlighted several aspects about the fiberglass and epoxy-resin mix. The fiberglass itself did not fail or crack during the entirety of the test. The epoxy-resin mix began cracking at the 9 mm displacement mark and 611 lbs, but continued to hold its structural integrity. Two more slips occurred at the 9.5 mm displacement mark and at around 9.65 mm with 1150 lbf and 1400 lbf respectively. Both of these followed a similar pattern where the plate was still held in place without issue for the test. At just after 10.5 mm of displacement and 2170 lbs of force applied upon the plate, the epoxy-resin mix's integrity was compromised, and the plate slipped resulting in part total failure. However, since the maximum force of the L1000 motor upon the same surface area was only going to be 304.616 lbf for a brief second during the duration of flight,

a safety factor of 7.124 was granted, validating the design. Even if the plate had slipped at the 611 lb mark, it would still have still granted a safety factor of 2.006, which was the minimum that was required to validate this method.

Materials Selection

G10 fiberglass was chosen for the bulkheads due to its relatively lightweight properties in addition to its relatively high compressive strength of 55,000 psi. The bulkhead section will receive the lion's share of the compressive forces placed upon the rocket due to the motor's burn and the ejection charges. As a result, it was critical that a lightweight material with respectable strength characteristics was chosen. Aluminum and steel, while likely providing a strong structure that would be unlikely to fail, would have been prohibitively heavy. Plywood would have been incredibly light, but with a compressive strength of, at most, 6,000 psi, it was questionable whether or not it would be able to withstand the proper forces. As a result, a middle-ground solution in the form of G10 fiberglass was used since its weight characteristics were only marginally larger than plywood while providing vastly greater structural integrity.

Manufacturing

The bulkheads were manufactured on the TM2 using a fixture plate to hold each bulkhead down such that a circle could be cut without numerous fixturing operations. 0.25" G10 fiberglass was cut into 4.25" x 4.25" sections and marked at its center so that a datum could be created from this position. Initial plans required a single 0.5" hole at the center of the bulkhead. This hole will be the mounting point for the eye bolt and paracord for the parachute. In order to fixture the bulkhead for the machining process two offset mounting points were needed. This was due to the fact that

if a single fixture, placed in the hole for the eye bolt, would allow the part to spin around the fixturing axis. As a result, two smaller holes spaced 0.5" apart across the center would allow for a superior hold. These holes would end up being wire pass throughs for the ebay. Afterward, a centering drill was used to mark the middle of the plate and a frame program was written in order to draw the circle. A 0.5" drillbit was used to mill a circle in two 0.145" depth cuts into the plate. A respirator was worn by the operator and a vacuum was held against the drillbit in order to prevent the fumes and fiberglass dust from being breathed in. The part had to be deburred and was fit into a piece of airframe test section. After this part was made it was determined that the "extra" holes used to fixture the bulkhead down may create structural weak points. For this reason a separate process was completed for the bulkheads which experience forces by the parachutes.

For these pieces, it was thought that the parts should be milled on the TM-2 mill with a single hole at the center. To solve the rotation issue two clamps were used to secure the fiberglass plates to the baseplate at each corner. A 0.25" drill bit was used to drill a hole into the center of the part. Afterward, a screw and washer were used to secure the fiberglass in place while the clamps were removed. A program was then written on the machine's interface to drill out a circular shape with the same 0.25" drill bit in three passes.

Fins

Design

The primary purpose of a fin is to provide a method by which to keep the rocket in a vertical state. This is achieved through the use of atmospheric drag and lift on an airfoil or fin. Two primary factors are considered in fin shape: cross sectional shape and profile shape. Examining the

45

dynamics of a high-power rocket and the relationship between stability and cross-sectional shape, we determined that using a more complex cross-section did not provide enough of a benefit to justify higher costs and complexity. In general, increasing the lift of a fin provides stability by spinning the rocket. Spinning adds an angular momentum component to flight that is very resistant to change, thus the rocket is more likely to stay in the vertical configuration. For higher velocities however, this does not hold true. At higher velocities atmospheric drag on each fin results in larger forces perpendicular to the flight direction. Thus, the added stability from the lift provided by the non-rectangular cross section does not justify the significant costs added to the project. Additionally, a greater degree of horizontal atmospheric drag will be seen on the fin given movement in the horizontal direction. This additional drag is sometimes referred to as attack angle drag. The rectangular cross-section does not experience this horizontal drag throughout the entire flight because the fins will not move through that volume of air perpendicular to the fin due to their inherent shape. Since this added induced drag can be avoided, our fin design, which does not include a non-rectangular cross section, should be able to reach higher velocities, further increasing the stability and final apogee.

The second component that we considered when designing a fin was the lateral or profile surface area needed to provide enough lateral atmospheric drag and move the CP back, relative to the front of the rocket. Generally, the surface area needs to move the CP back by one to two calibers. For our rocket, which is four inches in diameter, this means we need to move the CP back 4 to 8 inches from the CG. After analyzing the weight distribution of our rocket, the final fin length and height parameters were settled on. A fin length of 7" and total height (protruding from the rocket body) of 2.7" was created. A linear progression from 0" until 2.7" was carried for the leading edge until

the 2.5" mark. This 2.7" height is maintained until the 4.5" mark, at which point the height of the fin is reduced back to 0" by the final 7" mark. This geometry marks the final finest shape and sizing parameters.

Finally, the last factor considered was the leading-edge taper. Applying a 45-degree taper to the leading edge, according to the references, significantly decreases overall drag and aids the rocket in reaching higher velocities. This further increases the stability of the rocket in flight and allows the rocket to achieve a higher apogee. Given the summation of these properties and the final finest were manufactured such that they could be installed onto the rocket body.

Analysis

Research into fin designs and shapes has been conducted on a variety of lower velocity rockets, however, it is limited in the realm of high-power rockets. As such, we decided to conduct our own fluids studies on a variety of shapes to determine the best shape for our needs. When considering our third parameter, shape, our starting point was in identifying basic shapes of a rectangle, pyramid, trapezoidal, parallelogram, cropped delta, and an elliptical shape that have been used in other rockets. We decided, after initial research, to rule out the theoretically strong elliptical shape based on the understanding that our rocket will transverse between subsonic velocities and transonic velocities at motor burnout, for which the elliptical shape is not effective. Thus, Solidworks parts were made of the rectangle, pyramid, parallelogram, and the clipped delta fin shapes. In order to compare the different fins, a constant surface area of 6 inches squared was used as the control, as well as a velocity in the x-direction of 400 [m/s], and a constant air density of 0.95815 [kg/m^3], present at 2500 [m]. Each fin was put through a fluid simulation study to

determine its performances within the parameters of pressure, turbulent intensity, and temperature. Figures 20-25 show the turbulent air flow after the lagging edge of the fin.
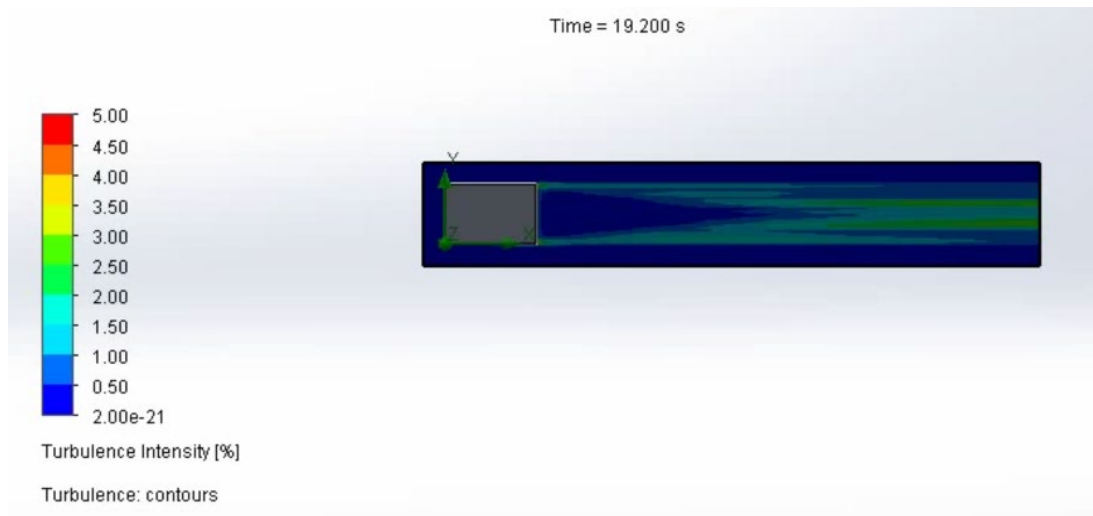

Figure 20 - Rectangular Turbulent Intensity
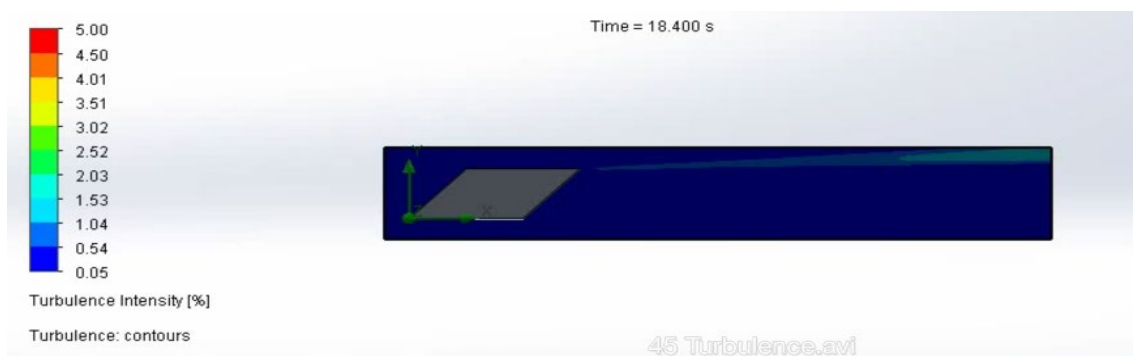
Figure 21 - 45 Degree Parallelogram Turbulence
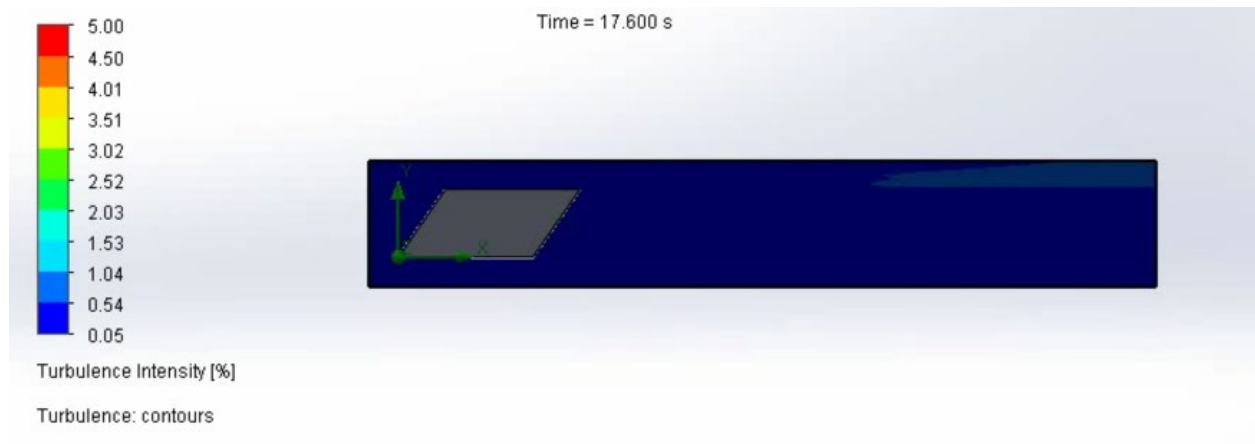
Figure 22 - 35 Degree Parallelogram Turbulence
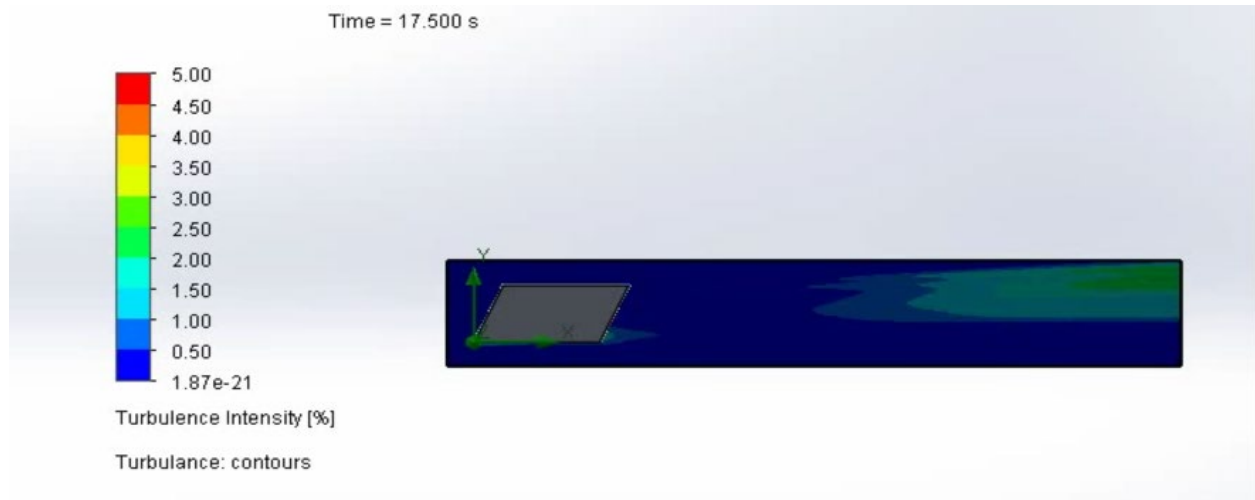
Figure 23 - 25 Degree Parallelogram Turbulence

49

Figure 24 - Cropped Delta Turbulence
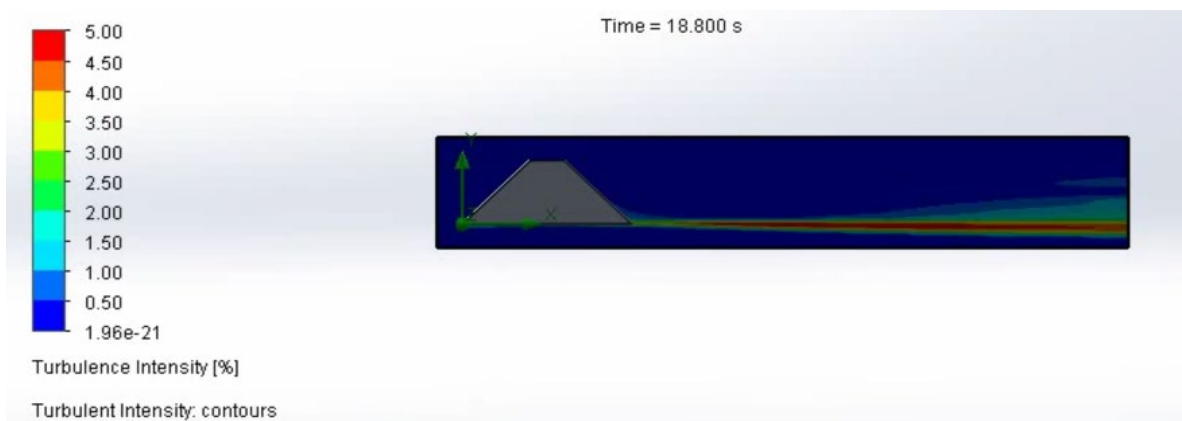
Figure 25 - Trapezoid/Pyramid Turbulence

Since the frontal area and surface area for each fin was maintained to be the same, shape is the driving factor when considering the drag induced by vortex shedding and skin friction. In general, minimizing the number of areas at which discontinuities of shape occur, decreases drag. This can be achieved by maintaining contact of the fin to the body tube through the length of the fin. Analysis of shapes and figures shows that the trailing edge will be in contact with the rocket body

50

for only three instances: rectangle, clipped delta, and the trapezoid. Interestingly for some of these shapes, vortex shedding does not always get condensed and result in a more streamline design but actually increases drag. The only shape to reduce drag overall is the trapezoid design, which can be seen in Figure 25. Further analysis reveals that the turbulence caused the shape would be moved to the rocket body, therefore reducing drag. This can be observed in the comparison between figures 23 and 25, where vortex shedding is moved from off the body tube to the body tube. It should be noted that although the turbulence is relatively larger in magnitude on the trapezoid design, it results in less drag because the flow will be moved to the body tube.

Based on the analysis of these figures, specifically looking at the magnitude and duration of vortex shedding, it was determined that the parallelogram or clipped pyramid produced the best shape performance. Additionally, this shape can vary in design through the adjustment of sweep angles, allowing it to be further optimized for efficiency at both subsonic and supersonic velocities.

Thus, a final shape design was decided upon. This design modified from the initial CFDs encompasses the best parts of both the Parallelogram and be optimized for the transonic-supersonic range. For the leading edge, a 45º angle, from vertical, is being used in order to reduce the frontal area of the fin while maximizing the efficiency in both the subsonic and the supersonic regions. The trailing edge features a 35º angle, from vertical, and will be used to minimize vortex shedding along that lagging edge. Given this design for the fins, based on the shape parameters tested, calculations were done to analyze the stresses and final drag coefficient on the fins with the body. Solidworks data, for this type of high-fidelity calculation, does not output accurate enough data to rely upon. Thus, in order to obtain higher fidelity results, calculations were performed based on

the equations and data found in *Tactical Missile Design* by E Fleeman. Equations 3-5 and were used to calculate the drag coefficient for the body and Equations 7-8 for the fin drag coefficient.

$$\left(C_{D_0}\right)_{Fin,Friction} = n_{Surface}[0.0122 \left[\frac{M}{qC_{mac}}\right]^{0.2} \left(\frac{2S_{Surface}}{S_{Ref}}\right) \qquad Equation\ 7$$

$$\left(C_{D_0}\right)_{Surface,Wave} = n_{Surface} \left(\frac{1.429}{M_{\Lambda LE}^2}\right) *$$

$$\left\{(1.2M_{\Lambda LE}^2)\{1.2M_{\Lambda LE}^2)^{3.5} \left[\frac{2.4}{2.8M_{\Lambda LE}^2 - 0.4}\right]^{2.5} - 1\right\} *$$

$$\left\{\frac{sin^2\ \delta_{LE}cos\Lambda_{LE}t_{mac}b}{S_{Ref}}\right\} \qquad Equation\ 8$$

Equations 9-10 were used to calculate the normal coefficient on each fin, where equation 9 is the normal force on the fins and equation 10 the normal force on the body.

$$\left|(C_N)_{Surface}\right| = \left[\left(\frac{\pi A}{2}\right)|sin\alpha' cos\alpha'| + 2\ sin^2\ \alpha'\right]\left(\frac{S_{Surface}}{S_{Ref}}\right) \qquad Equation\ 9$$

$$(C_N)_{Body} = sin(2\alpha)\ cos\ (\alpha/2) + 2\left(\frac{l}{d}\right)sin^2\alpha \qquad Equation\ 10$$

Table 1, shown below, shows that the drag coefficient for a fin including wave drag, base drag, body drag is 0.762. and that the normal force coefficient on each fin is 7.774 based on body and tail (fin) components.

Parameter	Value
C_D	0.8609901843
C_N	20.87082044

Table 1 – C_D/C_N Calculations

FEA

Complex geometry and mating surfaces between each of the fins and the body tube required a different method of calculating deformation and forces imparted. In this rocket each fin will be made of a fiberglass sheet, cut to the appropriate size and re-cured to retain the same strength characteristics as the manufacturer specified. This method was used to ensure that strength characteristics are the same regardless of if we manufacture the fins from scratch or if we buy sheets and cut them to shape. For this simulation the fins, most aft body tube, and motor casing were used. However, these parts are all held together with epoxy. To best approximate the epoxy connection between each individual part a Solidworks weld fodder was created between the appropriate parts. Solidworks does not allow for faces that do not contact one another to have force transfer between them or to have weld fodders between them. Thus, due to the rectangular cross section of the fins and the circular cross section of the motor casing, the sizes of the motor tube and fins had to be adjusted such that faces made complete contact. After adjusting the faces of each part so that they contact one another, forces were then applied to the fins. Similar to the forces being applied on the nose cone, the force will be applied parallel to the body tube and onto each of the fins. Because of the low Mach number there is no concern for shock waves impacting the fins or any part aft of the nose cone. Thus, the magnitude of the force calculated in the fluid simulations for these fins was applied in the direction specified above. Accounting for a safety

factor of 2 this final force of 480 N was applied parallel to the body tube. In order to maintain equilibrium, the motor casing was fixed in place on its outer surface and lower cross section along with the aft section of the body tube. This will allow the fins to apply forces to the body tube and deform along their internal axis such that we can evaluate the likelihood of failure on the epoxy welds and movement associated with wind force. The final mesh was created at the highest fidelity possible for thin walled FEA simulation. Element size was set to 0.5" and the tolerance to 0.025". The mesh has 28,988 nodes and 14,127 elements. This study was conducted with a 16-point high-quality Jacobian mesh. 87.649% of elements have an aspect ratio between three and 10. No elements were distorted in this mesh. The final result of this FEA simulation revealed a maximum deflection of $4.395 \times 10^{-3}\ mm$ of deformation. This deformation is less than the part tolerance when manufactured. Thus, the conclusion was reached that the parts will not fail during flight. Figure 26 below is a visualization of the stresses on the rocket body and fins given the force profile.
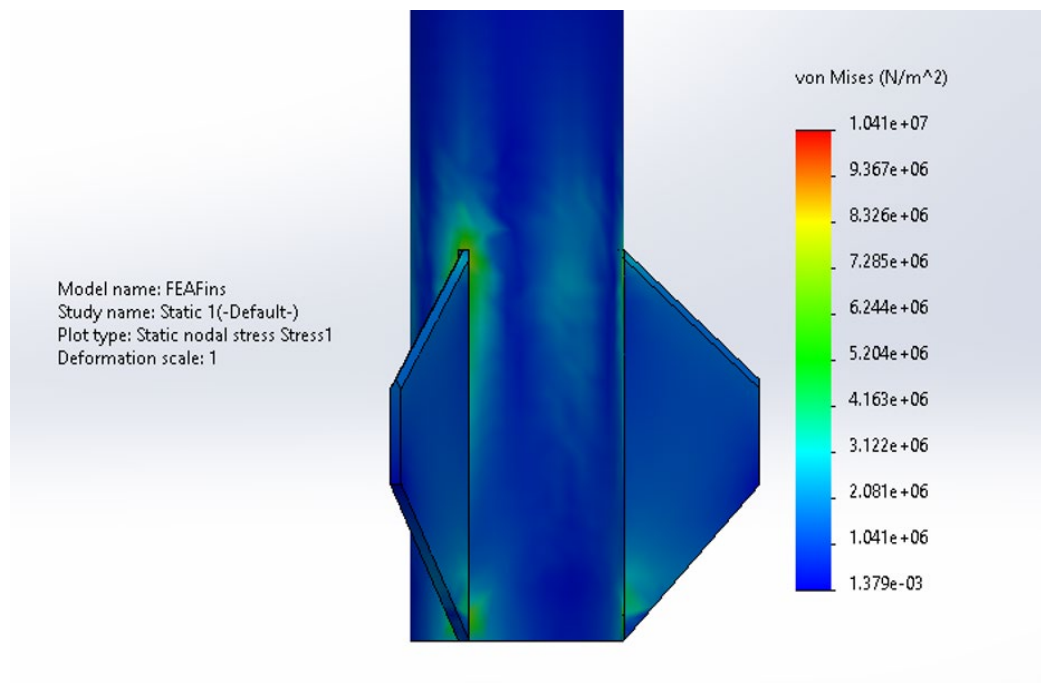

Figure 26 - Fins von Mises Stress

Materials Selection

When considering the materials for the fins the primary factor is weight. Since the fins won't experience a large degree of force due to the inherent stability of the rocket, they do not need to be made of a material with a high shear strength. Given this consideration, two main options were considered: plywood and fiberglass. Since weight is the primary concern, the density of both materials was weighted most heavily. Plywood can have a density ranging from 400-700 kg/m^3 and fiberglass a density of approximately 50 kg/m^3, making it significantly lighter. Thus, the fins will be made out of fiberglass.

Manufacturing

The fins were manufactured on the TM2 using an ⅛ end mill and a 90-degree end mill to achieve the dimensions and shape parameters required. Each fin was mounted to the cutting bed using toe clamps on the factory edge of each fiberglass sheet. The clamps were placed such that they would not need to be moved in the middle of the cut, requiring the machine to be stopped, creating additional unnecessary error. The trailing x-axis and y-axis edges were used as datums since they would be factory edges throughout the entire milling process. To prevent part fracture or other unexpected consequences the fiberglass sheet was cut in two, half-depth, passes. The machining process for this part started with milling out the rough shape of each finest with an ⅛" end mill. Once the shape was milled, the tool was switched with a 90-degree end mill. This tool milled out the leading edge of the finest creating half of a 45-degree taper. After this pass the finest was flipped over so that the other half of the taper could be cut. Once all three cuts had been made the process was repeated for three other fins. This brings the total fins created to four. Since the

designed rocket only has 3 fins in its finest, the fourth was created as an "extra" part which could be used if any of the parts were out of tolerance.

Parachutes and Paracords

Design

Two sets of parachutes are to be used in the rocket design such that one parachute may be used to slow the descent speed enough that the rocket does not free fall to the ground, and one to slow the rocket to its final descent rate. Since the rocket will be flown in the high velocity wind conditions of Kansas the drogue parachute must not reduce the descent rate of the rocket too much, causing excessive drift. Based on the recommendations of expert rocketeers a desirable drogue descent rate is approximately 85 ft/s. Given our expected rocket weight this descent velocity would be achieved with a parachute diameter of 2'. Similarly, the desired decent rate for the rocket is less than 30 ft/s. For our rocket this can be achieved with a 4' parachute diameter. This will yield a final descent rate of approximately 25 ft/s.

Analysis

1. Main Parachute

The main parachute was designed such that the final descent velocity would be at most 30 ft/s. In order to achieve this a 4' diameter nylon parachute was equipped. Given the parameters of the parachute needed, calculations concerning the forces applied on the bulkhead were done. Open rocket was used to determine the acceleration of the rocket during the main parachute deployment. Given this, and assuming a found acceleration of 59 ft/s2 for one total second, and assuming the weight of the rocket to be 15 lbf, the force applied on the bulkhead was calculated using Newton's

56

second law. Given a safety factor of two the force on the bulkhead was 85lbf. This force was used in the FEA featured below.

The mesh and calculations for the main parachute and bulkhead were done with a 16-point High-Quality Jacobian mesh. The mesh contained 57,409 nodes and 33,604 elements. Each element was 0.0079005 m with a 0.00039025 m tolerance. The maximum aspect ratio for the elements in this mesh was 8.2909 and 97.4% of the elements had an aspect ratio below three. The maximum deflection observed for this bulkhead and eyebolt was approximately 0.9 mm or 0.0354 in. This is a minimal deflection concerning the scope of this design and is considered acceptable given the safety factor.
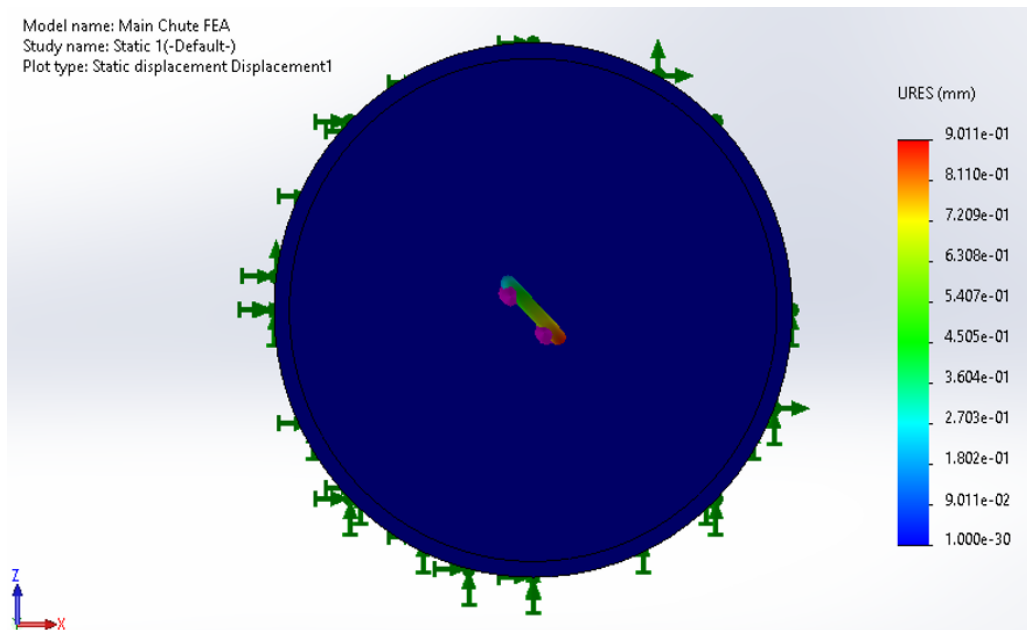

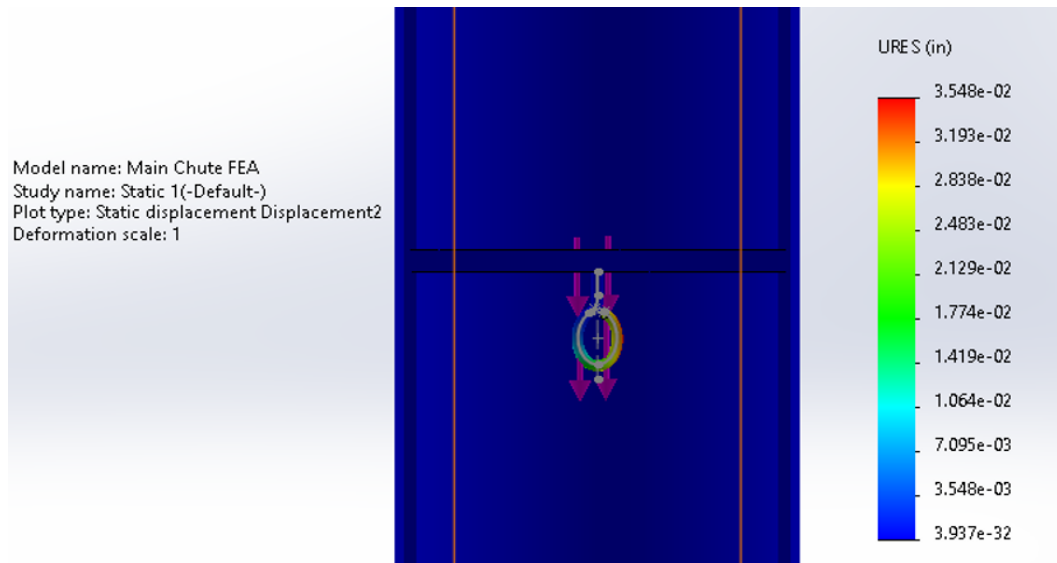*Figure 27 - Main Parachute Deflection (Top)*

Figure 28 - Main Parachute Deflection (Side)

2. Drogue Parachute

The drogue parachute was designed such that the descent velocity for the post apogee and pre main parachute deployment would be at most 100 ft/s. In order to achieve this a 2' diameter nylon parachute was equipped. A 2' parachute will slow the rocket to 85 ft/s for this descent section. Given the parameters of the parachute needed, calculations concerning the forces applied on the bulkhead were done. Open rocket was used to determine the acceleration of the rocket during the main parachute deployment. Given this, and assuming a found acceleration of 17 ft/s2 for five total seconds, and assuming the weight of the rocket to be 15 lbf, the force applied on the bulkhead was calculated using Newton's second law. Given a safety factor of two, the force on the bulkhead was 46lbf. This force was used in the FEA featured bellow.

The mesh and calculations for the main parachute and bulkhead were done with a 16-point High-Quality Jacobian mesh. The mesh contained 67,407 nodes and 33,602 elements. Each element was

58

0.0079005 m with a 0.00039025 m tolerance. The maximum aspect ratio for the elements in this mesh was 7.0589 and 97.4% of the elements had an aspect ratio below three. The maximum deflection observed for this bulkhead and eyebolt was approximately 0.5 mm or 0.0197 in. This is a minimal deflection concerning the scope of this design and is considered acceptable given the safety factor.
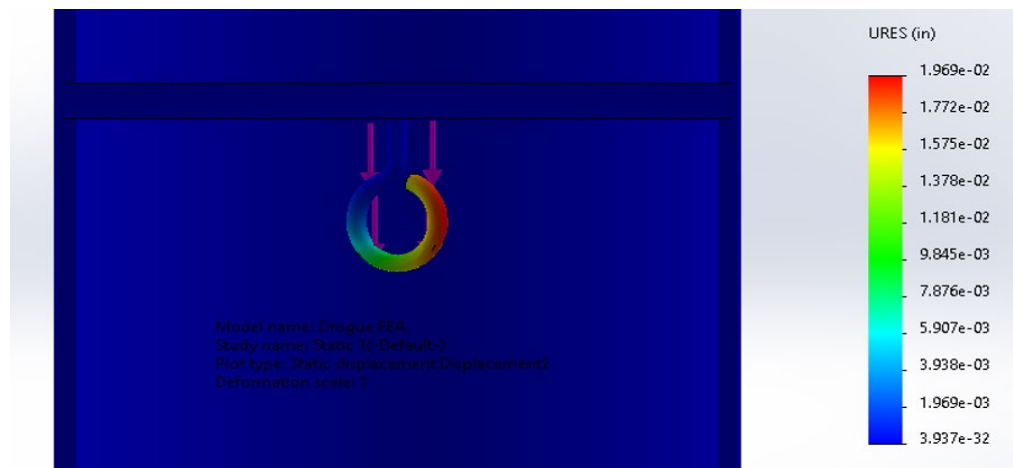

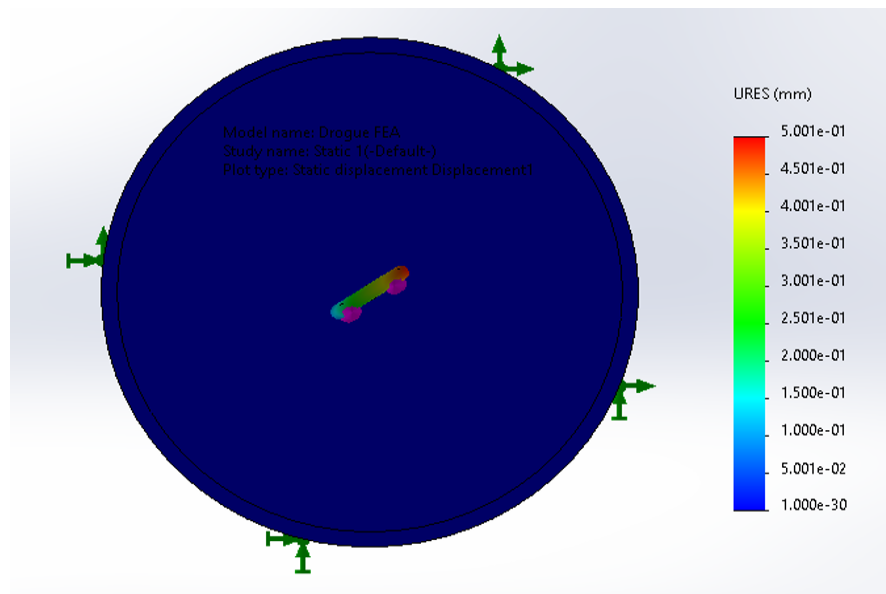*Figure 29 - Drogue Parachute Deflection (Side)*

Figure 30 - Drogue Parachute Deflection (Top)

The free body diagram used for both parachutes can be seen in the figure below.

Figure 31 - Parachute FBD

Materials Selection

The parachute design chosen is nylon, which offers stellar wind resistance, favorable elasticity, resistance to mildew, and its relatively economical characteristics. In addition, nylon parachutes are accessible as they are a common COTS product that is lightweight. They also offer exceptional robustness, and are resistant to abrasion and chemical contact, which is ideal when considering a design that could potentially be exposed to the rocket's ejection charges.

Manufacturing

Given the material choice for the parachutes and shock cords the *Polaris Rocketry* team will be purchasing both components off the shelf. Manufacturing a large nylon parachute is not something that the hub is currently capable of doing. Additionally, we do not have the expertise to do so. Similarly, the hub does not have the ability to produce high strength Kevlar braids for the shock chords. Given these factors both the parachutes and shock chords have been purchased

commercially. Given the final calculations that were done for the main and drogue parachutes 4'
and 2' nylon parachutes were purchased from Apogee Rockets. Additionally, 0.230" #1500
braided Kevlar cord was purchased for the shock cords.

Payload Section

Design

There were major design changes over the transition between the first and seconds that took place
on the quadcopter/payload delivery system. It was determined that the solution chosen for the
previous semesters design would not allow us to maneuver the quadcopter with sufficient control
for the needed purposes. Testing revealed that the electrical speed controller units were too heavy,
the motors being used drew too much power, and most notably there were not enough UART
registers available on the Arduino nano for all the components planned on the payload delivery.
Thus it was determined that an electrical redesign would be necessary for the purposes of the
competition. In order to achieve the competition goals a printed circuit board that had onboard
electronic speed controllers and a way to function them at a high amperage allowing power to go
to the motors in operation was needed. A DC motor that was small but packed a large torque output
in order to lift the heavy payload under minimal weight to thrust ratio was also needed.
At the beginning of the design process the proposed and targeted final drone weight would be
around 1kg. In this case the lighter the better, however this would serve as a baseline for
component selection. In order to achieve the desired acceleration goals a motor selection that
would provide at least a 1:1 lift to thrust ratio was required. More thrust than this was not
necessary as this payload will not be designed to make quick maneuvers or acrobatic flight
patterns, thus reducing the required thrust to weight ratio. The decision was made to use a 2205

2300KV Brushless Motor CW/CCW configuration as it was able to provide a Max thrust of over

1 kilogram and had a max current of 27.6 amp hours. This creates a total 110.4 A max draw at

maximum thrust, reasonable for the delivery system application. The physical specification of

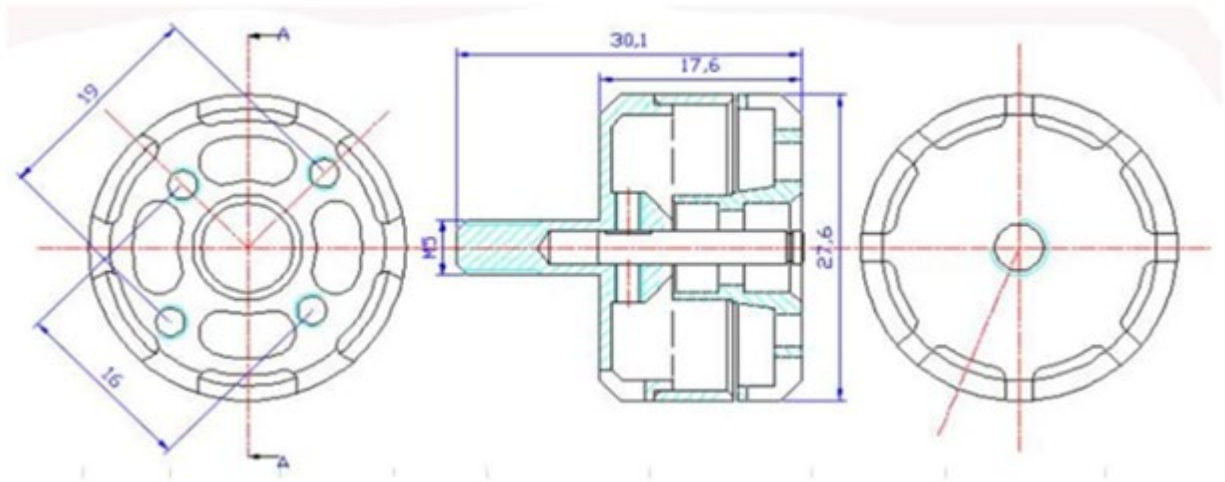the motor can be seen below in figure 32.

Figure 32 - 2205 2300KV Brushless Motor CW/CCW

Knowing the max current rating on the motors a battery selection on the quadcopter could be

further defined. The main criterion for this battery is that it needed to have a high capacitance

discharge rate that would allow the max current draw to hold and not provide overcurrent in full

power draw. This power draw, if exceeded, could render the battery useless in flight and drop our

payload from its flight path. All four Motors combined the maximum proposed current draw

would be around 110.4 AH. In calculation, it was found that many batteries will work but it was

decided to use a 1300mAH 120C battery as it satisfied our requirements. It is also worth noting

that three celled Lipo batteries were chosen when considering weight and voltage ratios. The final

battery chosen was a 11.1V 3S 120C 1300mAH battery for the final design of the drone.

Additionally, a flight controller board that was fully programmable and met all the required specifications in the F722 AIO 35A 2-6S development board was found. Most notably, this Control Board had a 35A rated electrical speed controller that would support the maximum torque of the Motors at 26.5 amps. With an amp rating so high the payload would be able to deliver maximum thrust to the motors with no extra weight added from external electrical speed controllers. Along with having this capability, this flight control board came complete with six UART registers that would be able to hold the GPS module, the camera module, the receiver for I-Bus transmission to the flight controller, and two extra UART pads for any other design changes that may result from further testing.
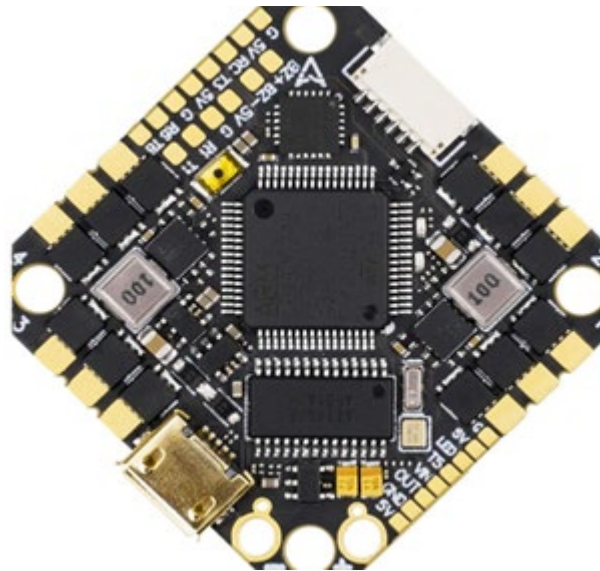
Figure 33 - F722 AIO 35A 2-6S Flight Controller BLHELI_32 35A ESC No RX with XT60U to BAT connector

The next goal was to find a way to control a quadcopter remotely using a receiver and transmitter setup. Looking into viable transmitter and receiver options proved difficult when also considering the limited available budget. Due to the limited use that this drone would be used for it would only need to transmit on the ground in order to tell the flight controller to beacon at home and find its

63

way point. This means a maximum 100-meter transmission range, to reach the quad when sitting on the launch pad, and a maximum 300 meter transmission range, to reach the payload in flight and gain control of the quadcopter once the payload was deployed from the rocket apogee, would be needed. Thus it was decided to use a 6-channel transmitter that had an I-Bus configuration. An added benefit of which is that it is able to take only one of the UART pads on the flight controller. This inverted bus signal would be used to transmit to a controller on the ground.
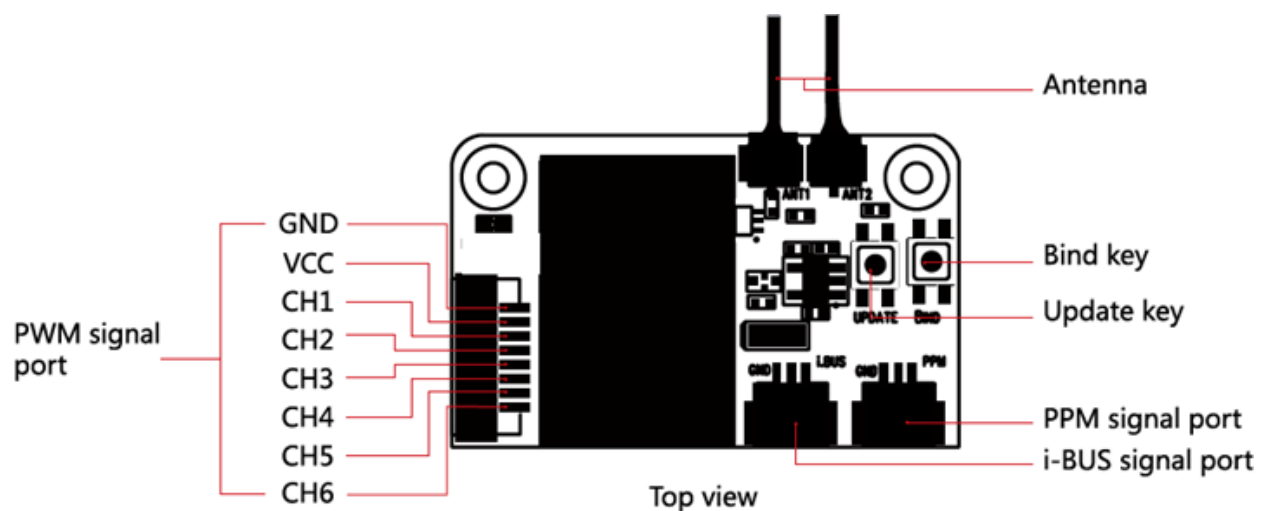
Figure 34 - FS-X6B Receiver 6 CH 2.4G i-Bus PPM PWM Receiver for AFHDS i10 i6s i6 i6x i4x Transmitter

A cheap transmitter in the Flysky application was found. In research, it was also discovered that the firmware was alterable such that the transmitter could be improved to fit the competition needs. In factory mode this was only a 6-channel transmitter. However, given the firmware and software changes made, this controller could be used as a 10-channel transmitter. These changes were accomplished with a re-program of the machine language which was replaced with custom designed code.

Figure 35 - FS-i6 AFHDS 2A 2.4GHz 6CH Radio System Transmitter

Now that the setup process and design was completed, it was now time to program the controller and figure out how the payload design would work in flight. The first task was to figure out how to control the roll-pitch-yaw-thrust settings, configure the flight controlle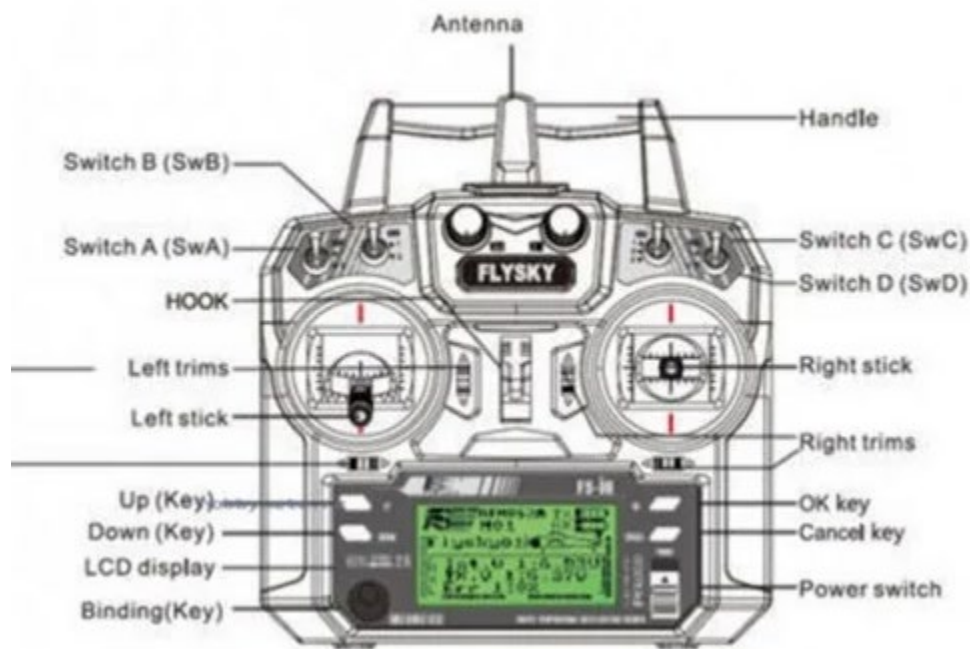r, and set the endpoints of the transmitter and receiver. In doing this endpoint set, the gimble (sticks) is given a tighter more responsive layout over the flight pattern. It was found that the cheap transmitter came with some fallbacks, as the gimble sticks on the circuitry were off by a 0.5% error rate. This error proved too great and needed to be compensated for in our design. It will also need to be overcome for flight and when deployed out of the rocket.

After considering the electrical components of the Payload Section, the mechanical components needed to be considered. Although the basic principle of the Payload Section has stayed the same, many of the details have changed. Figure 36 below is an illustration of an early design. Some of

65

the key features that have changed since this design include; the golf ball retention system, articulating arms, arm retention system, and electronic bay(s).

Figure 36 - Preliminary Drone Design

The evolution of this design has led to the definition of a few key features. 1: The propellers, both in regard to size as well as location and number, 2: the body diameter relative to the rocket, 3: the golf ball retention system and 4 the electronic bay(s). Key feature 1, the propellers, was an easier aspect of this design once the motor was selected. As stated previously, the original motors that were selected were very weak and did not provide sufficient thrust. Thus, a three-blade system was designed to provide additional thrust for low motor RPM. However, the later selection of the motors allowed for a reduction in blades to two blades per motor due to the increased capability of the motors to spin faster. Key feature 2, body diameter, was decided upon early in the design process and was a key design limitation for the entire quadcopter design. Since the rocket itself would have an inner diameter of 4" the drone itself must have a smaller diameter as well. Thus,

66

the drone was designed to be 3.95" so that a smooth yet loose fit would be present. Key feature 3, the golf ball retention system, went through two main design iterations. The first being a loose pin and slot system which relied on long all-thread to hold the system in place. This design was not ideal as it did not consider weight and resulted in the golf ball having too much room to move about. Thus, a second design was created. This design features an undercarriage cup which holds the golf ball firmly on all sides and presses upon the bottom of the electronics bay, keeping everything firm and lightweight. Key feature 4, the electronics bay, went through the most changes. Given the spacial challenges of having the drone fit into such a small space, issues arose with fitting electronics inside the body of the drone. This meant that the majority of the electronics would be moved to the top of the drone such that they could lay flat and not occupy the space where the propellers and motors would need to be. The final iteration of the drone features all of these changes and can be seen in figures 37 and 38 below. Where figure 37 is the Solidworks model and figure 38 is the actual manufactured part.
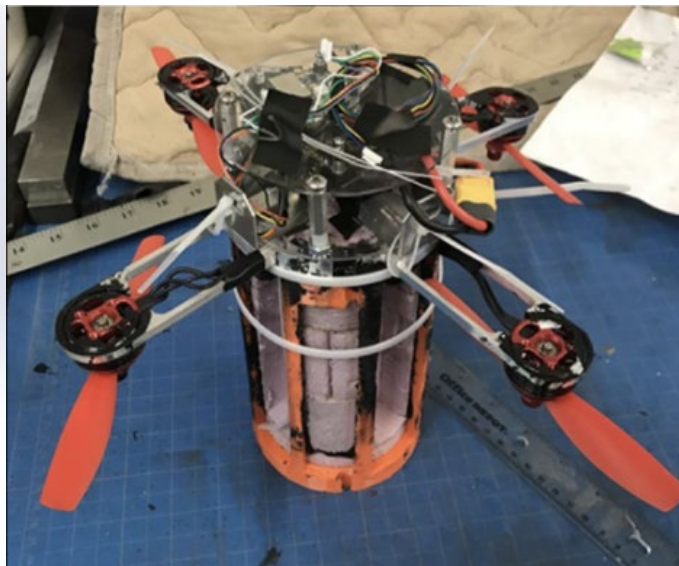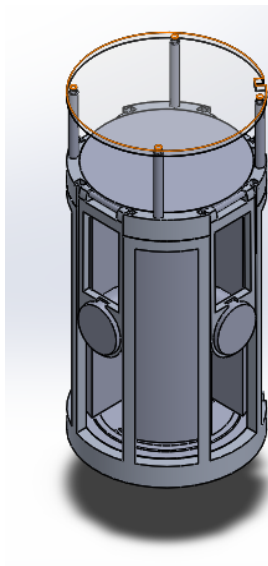
Figure 37 – (Right) FS-i6 AFHDS 2A 2.4GHz 6CH Radio System Transmitter

Figure 38 - (Left) Late Drone Design

Analysis

The no load graph below represents the ideal operation of the battery without load onto the circuit. Observing the graph, it can be determined that there is a large index of current applicable to a small voltage.
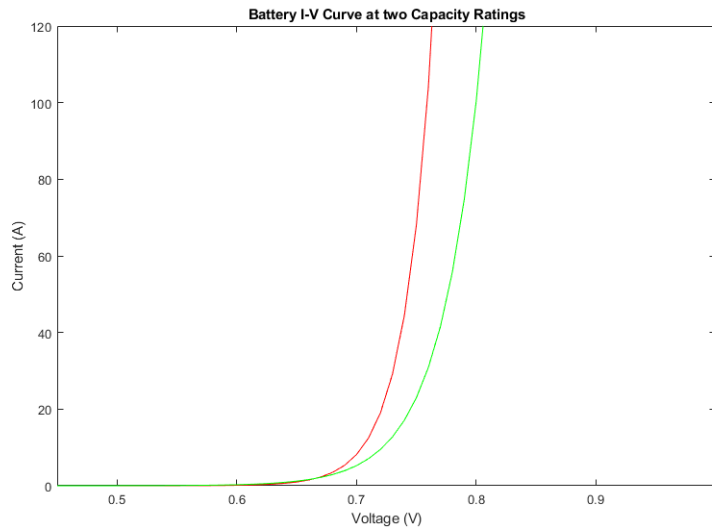
Figure 39 - Battery I-V Curve at Two Capacity Ratings

Additionally, a torque versus angular velocity graph of the motor shows that these potential motors are an excellent selection. They provide linear torque and speed for our application.
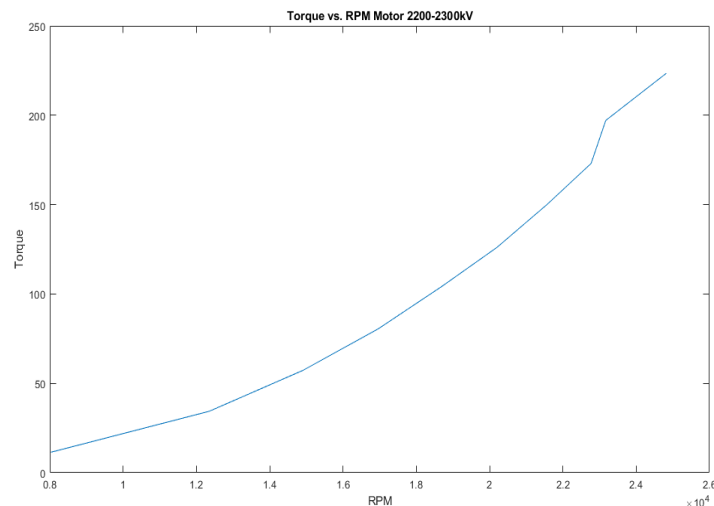
Figure 40 - Torque vs. RPM Motor

68

In order to lift the payload for flight a lift ratio of 1:1 on all four motors is required. The lift ratio was considered for all four motors at the desired rotational speed. It can clearly see that the RPM for lift is not even close to half of what the potential motor output is. With around 15000 RPM applied to each motor, the drone is able to successfully lift the payload if it is around 1000 grams or below. With this in mind, it is possible to almost double or thrust to weight ratio throughout flight.
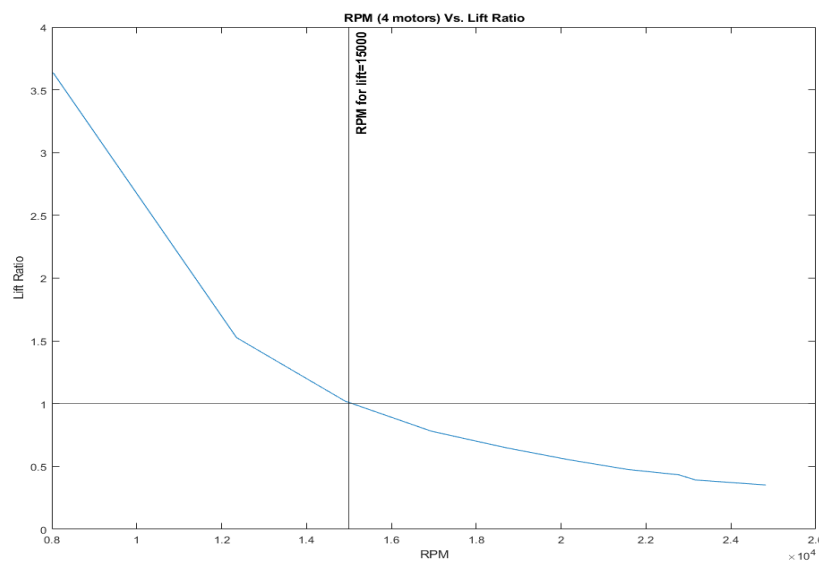

Figure 41 - RPM (4 motors) vs. Lift Ratio

The amp draw is plotted against the lift ratio in rotational speed in order to gain a better understanding of how much current draw is necessary to achieve the desired thrust to lift ratio of 1:1. Observing the graph it becomes apparent that at around 10 amps the motors will successfully lift the quadcopter for the previously plotted rotational speed. This is a necessary calculation because the chosen electrical speed controller is rated at 35 amps meaning that these motors are an excellent choice for the required application.

69
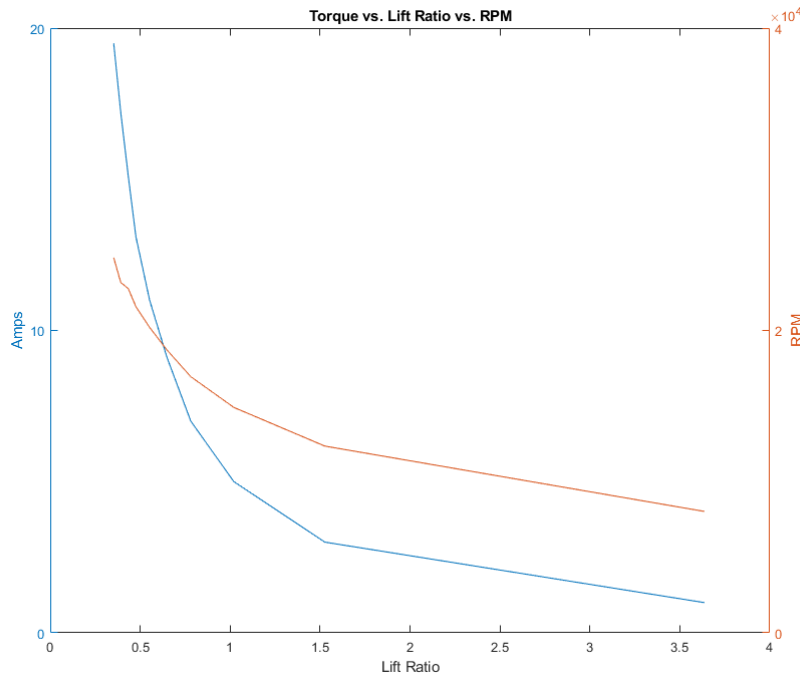
Figure 42 - Torque vs. Lift Ratios vs RPM

Materials Selection and Manufacturing

Materials selection for the payload proved to be very difficult. Most materials that are readily available and will provide sufficient structural support are very heavy. In the process of brainstorming suitable materials for the body of the quadcopter PETG was selected. At the time this material was thought to have sufficient structural stability to withstand flight forces and would be light enough to minimize payload weight. Additionally, the material is very easy to manufacture and allows for post manufacturing modifications with minimal cost or lost time. Thus, the decision was made to 3-D print the body of the drone.

After manufacturing one of the first iterations of the quadcopter body it became readily apparent that PETG was far too heavy and that it is very brittle. In order to save weight, the structure of the quadcopter was hollowed out into a "frame" leaving only essential structural components. Since

70

the material is very brittle without any other members of support, additional reinforcement was added. Since the majority of the drone shape was given by the PETG a foam insert was made for the interior cavity. This insert provided support for the walls of the drone while maintaining a light profile and ease of manufacturability.

With the main body of the drone complete the next step was to manufacture mounting points for the arms and to make the arms themselves. Since the PETG had experienced a lot of machining forces and was very brittle the decision was made to add aluminum standoffs to hold the pins in. Aluminum was chosen because it is relatively lightweight and can support itself as an addition to the pre-existing structure. It was machined so that the pins would sit as far back as possible and low enough that the arms would clear the top of the electronics bay. Once these components were finished the arms were made.

The arms were originally designed to be made out of PETG. This was because it was assumed that the infill could be reduced significantly enough to lighten the parts while still being structural. However, after testing and FEA it was determined that this would not be the case. To substitute, aluminum arms were manufactured which maintained the same basic shape and function. Since that material is so much heavier than PETG it was machine into a frame so that the motor was only held in by the minimal material required. The result actually ended being lighter than the original design and still held up to the design loads.

Finally, in order to articulate the quadcopter arms a spring and magnet retention system was designed. This system is designed to articulate the quadcopter arms from a vertical configuration,

for which they will fit in the rocket body, into a horizontal configuration, for which the flight will be carried out. The original design for this system used a single spring which was nested into the payload arm such that the spring would provide a torque on the hinge point of the arm and cause the arm to move from horizontal to vertical. This design, in principle, worked, however it did not provide enough support to serve as a final design. The reason that the design was not sufficient was in large part due to the fact that the spring was not strong enough. The reason that this is the case is that the available space in the quadcopter arm prevented a larger spring from being readily purchased. For this reason, a series of three springs per arm were added so that the total force applied increased threefold. The result of this modification was that each arm flexed to the required resting position. Unfortunately, they did not stay in this position and quickly fell back to a non-horizontal orientation. In order to fix this a second retention system was added. This system featured a set of steel shims and magnets which hold the arms up once they have been articulated. The shims were attached to the arm such that when they reach their horizontal orientation the magnets fully engage with the shims. Similarly, the magnets were mounted such that they would align with the arms once they are in a horizontal orientation. This design works very well when combined with the spring and ended up being the final design.

Motor Casing and Motor

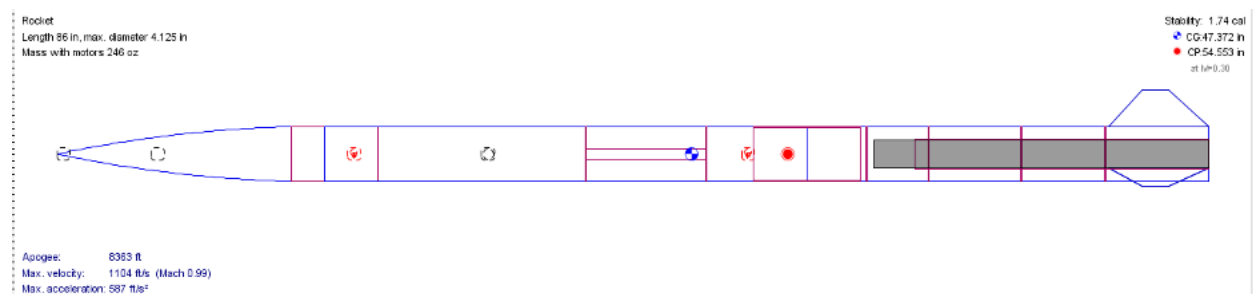### Design

Two motors were seriously considered when evaluating the rocket propulsion system, the K660 and the L1000W-18A. Both are Aerotech products that have high-regression designs, however one has substantially more power and impulse than the other. The K660 was primarily considered for its economical properties, given that the previous year's team had a motor left over and additional

72

motors would be cheaper. However, given a large payload that will be able to slow its descent enough to maintain control over the duration of the flight, the rocket needs more impulse to reach 8000' AGL. Thus, the L1000W-18A was considered for its higher impulse and shorter burn time. A comparison of the impulse of the K600 to the L1000W-18A shows that the L1000W-18A has a one second shorter burn time with an additional 247.4 N-s of impulse. Additionally, the L1000W-18A has 223 g more propellant mass than the K660. These differences mean that with the L1000W-18A we can reach an altitude of 8971' as opposed to 8481' with the K660 holding all other variables the same. Thus, we can increase the payload size such that it could drop our apogee by 500' without impacting the rest of our design in any significant fashion.

Analysis

1. Overview

For the purposes of flight profile simulations and for overall design, the software *OpenRocket* has been used. This software outputs a 2D rocket profile with block diagrams for components based on user component input. The flight configuration profile for this year's Argonia Cup Rocket can be seen in figure 43 below.

Figure 43 - OpenRocket 2D Profile

This configuration yields a stability of 1.74 caliber and a final apogee of approximately 8400'. This model, while physically complete, may not completely represent our true final altitude. Until components are fully manufactured, element weights, and exact dimensions are only estimates. It is important to note that many of the parts are complete, however small changes in incomplete parts will still have an effect on caliber. Each simulated component will be updated with its final dimensions and weights upon the completion of its manufacturing process. Once all components are finalized and in hand, a final simulation will be run to determine the true apogee according to an accurate *OpenRocket* simulation.

One of the limitations of the *OpenRocket* simulator is its thrust profiling capability. Default configurations for motors often contain over or underestimates of thrust performance, this depends on the motor in question. Upon purchase and receival of the motor, the real thrust profile was also obtained. Using this thrust profile and a .jar program, a new thrust ".eng" file was created for use in the open rocket simulation. Figure 44, below, shows the final product of the curated thrust profile, and the thrust profile that will be used in the final *OpenRocket* simulation.
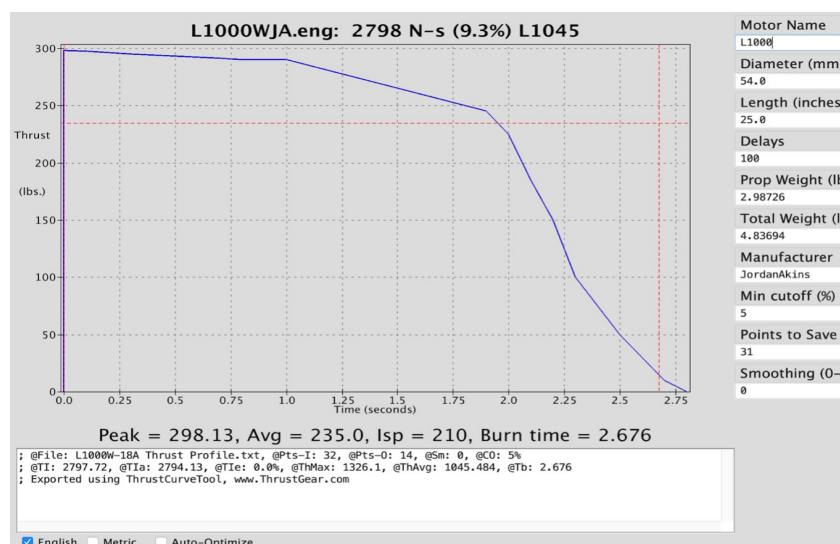

Figure 44 - L1000W-18A Thrust Profile

Analysis of the specifications sheet provided by the manufacturer allows us to calculate the maximum force exhibited on the rocket internals throughout the rocket flight. As shown in figure 45, our rocket will feature three centering rings and a motor retainer located at the lagging edge of the motor. Each of the centering rings will work in tandem to share the forces imparted by the motor and to maintain vertical equilibrium by concentrating all forces in the vertical direction. Each centering ring will be secured to both the rocket body tube and the motor inner tube through a high strength and temperature stable epoxy. Although the body tube and motor mount should not experience high temperatures, by design, and given the nature of high power rocketeering we will be using epoxy that can withstand higher temperatures as a safety precaution. As shown in figure 6, all three centering rings will be placed equidistant from one another and will be bonded to both walls in the same manner, in effect minimizing error.
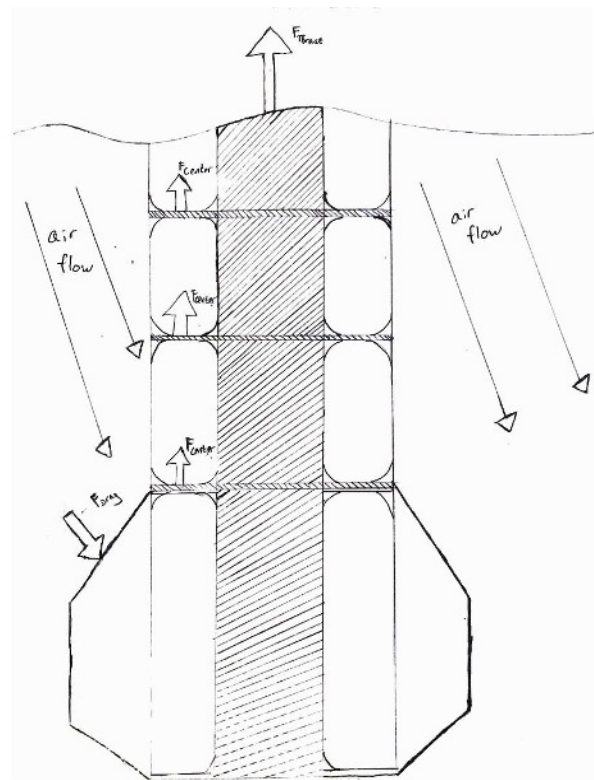

Figure 45 - Rocket Motor Attachment Free Body Diagram

Due to the cylindrical nature and thin profile of the rocket, the centering rings will need to be placed one at a time. Starting with the center ring we will pre-coat the outer diameter and inner diameter on both the top and bottom surfaces with epoxy. After the ring is coated, it will be fit over the motor and pushed to the final bond location. At this time a rod or stick will be used to apply additional epoxy such that a filet is created. This process will be repeated for the other two rings and the part will be set to cure for the next 24 hrs. This entire assembly will then be glued in, using a similar process, to the lower airframe section so that the motor is fixed in place on the launch pad and during flight.

2. FEA

Calculations for forces exerted on the bulkhead, which holds the motor mount and motor in place, were done assuming the maximum force given in the L1000W-18A product specification were the maximum forces on the component. Thus, the listed maximum thrust 1,355.2 N was doubled to account for a safety factor of two. A final applied force of 2,720 N was applied to the circular cross section of the bulkhead for which the motor would make direct contact. Further analysis of L1000W-18A thrust profile shows that for the thrust loading in this configuration we do not need to take into account any further forces. Any part which can withstand the maximum force, present at launch, will not fail for the duration of the flight. For this study, the forward edge was fixed in place such that the reaction force would be provided completely by the rocket body. Additionally, as a redundancy, the body tube outer surface was fixed such that no lateral (X/Z) deflection would occur. Placement of the bulkhead in the body tube was approximated for the "real" location in the rocket, however the exact location does not need to be specific as the body tube does not receive

significant force from the L1000W-18A. Examining the scale of the bulkhead relative to the scale of the body tube it became readily apparent that an extremely fine mesh would be required to achieve accurate results. Thus, a user defined mesh was constructed to provide the maximum number of nodes on the bulkhead, whilst minimizing the number of nodes on the body tube. The resultant mesh contains 61,998 nodes and 30,743 elements for which the maximum aspect ratio is 8.8195. 98.5% of nodes have an aspect ratio less than three. None of which are distorted in this mesh. The solid mesh was constructed from a 16-point high quality Jacobian mesh. The results of this study and high-quality mesh can be seen through a displacement mesh in Figure 46 below.
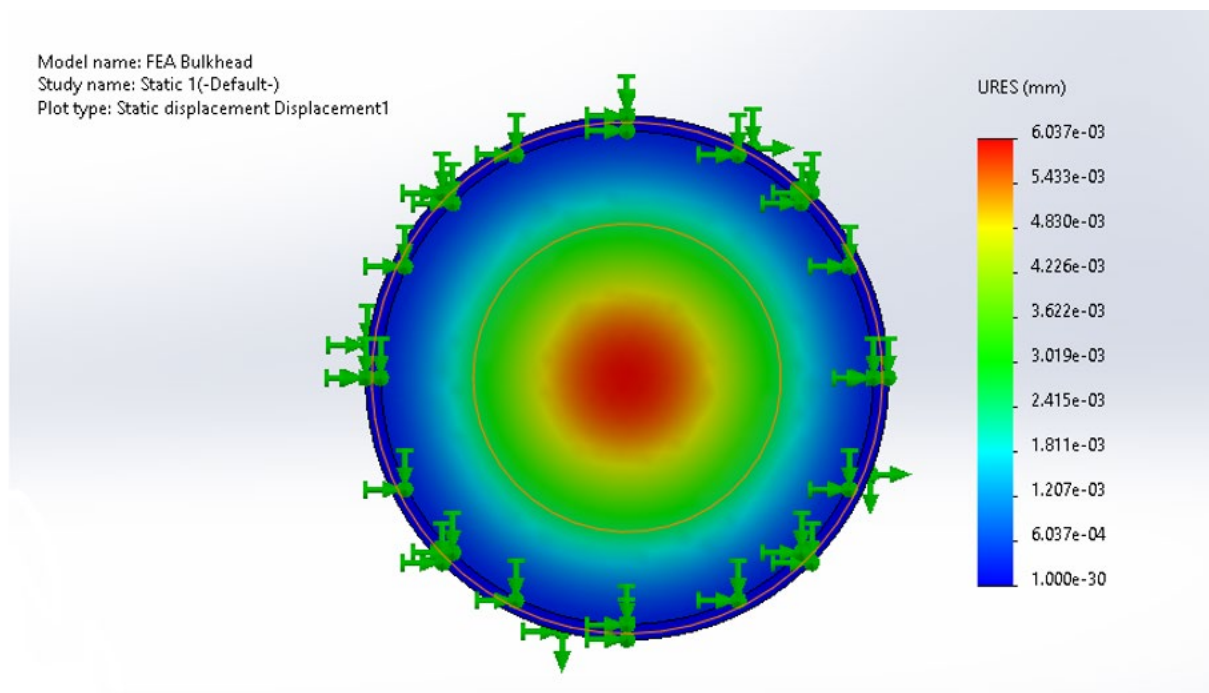

Figure 46 - Bulkhead Displacement

Detailed analysis of the bulkhead deformation plot reveals significant information about the structural stability of this bulkhead and system. The maximum observed deflection, located at the

77

center of the bulkhead, is approximately $6 \times 10^{-3} \ mm$. This deflection does not raise concern and is less than the tolerance to which the part was created. A primary assumption in the creation of this model is that the bulkhead is already attached to the body tube. When this rocket is constructed, the bulkhead will be secured with a high strength and thermally resistant epoxy. According to Figure 47 this epoxy must be able to withstand approximately a 21 MPa pressure. This will ensure, with a safety factor of two, that the bulkhead remains bonded to the body tube and not slip. Since strength characteristics for epoxy welds depend on filet size, the size of the filet will be calculated once an epoxy has been preliminarily selected.
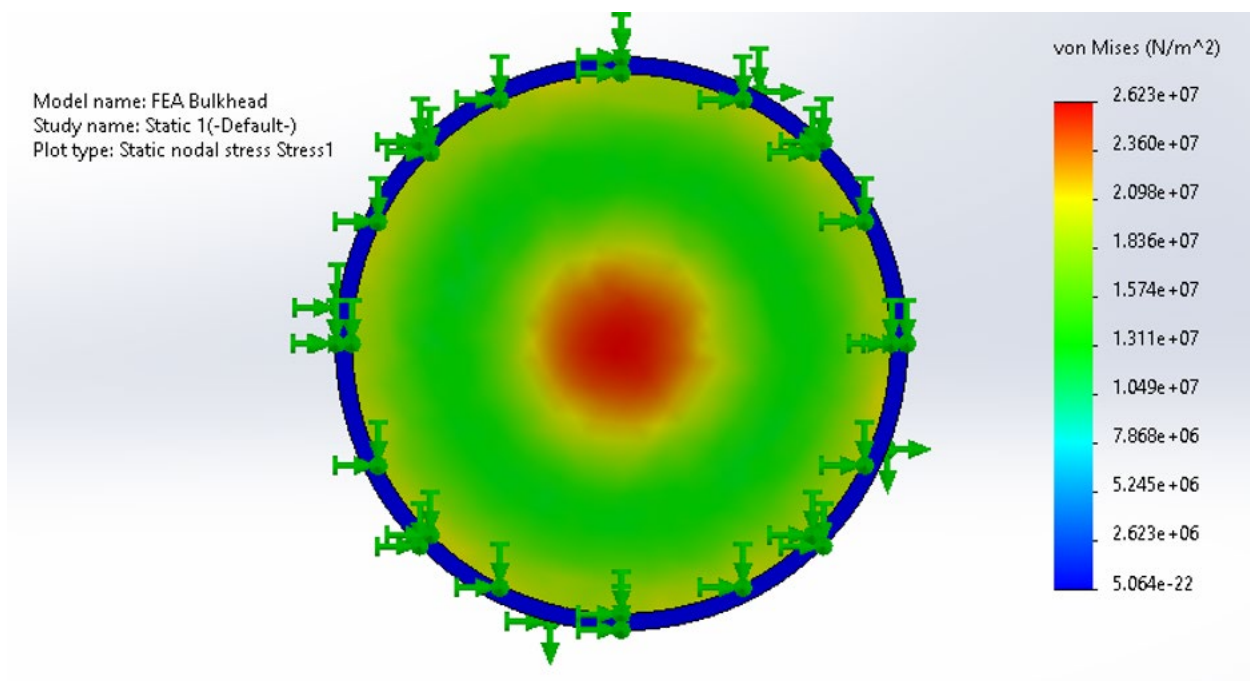

Figure 47 - Bulkhead von Mises Stresses

Materials Selection

For the epoxy that holds the fins, motor mount, lower bulkhead, and body tube together we used Proline 4500Q, a high temperature epoxy adhesive. This epoxy has a high thermal resistance such that it can hold under the harsh thermal conditions near the motor and strong chemical bonds such

that it can withstand the forces exerted by the motor during its maximum thrust burn stage. The bulkheads were made out of fiberglass and the centering rings out of plywood. The centering rings are made out of plywood to reduce weight while still maintaining stability of the motor mount. The bulkhead is made out of fiberglass because of its high strength characteristics and ability to withstand high temperatures if needed. The fins were made out of fiberglass so that they can withstand the compressive forces caused by the drag and any potential heat induced as well. A more detailed description of each of these components can be viewed in their appropriate sections.

Manufacturing

The first step for manufacturing the motor casing was to build a tool (mandrel) that could make a cylindrical part which could house the motor. Given the dimensions of the L-1000W-18A rocket motor, a mandrel was created that would accommodate a motor measuring 54mm (1.125") in diameter by 635mm (25.00") in length. A tolerance was also needed in order to fit the motor properly. It serves two primary purposes: The first was to facilitate the easy removal of the spent motor casing, post-flight. The second was to allow the necessary draft angle to exist on the tool to allow the simple removal of the part after it had cured. Due to the tight tolerances required to manufacture such a component, the lathe was selected as the tool to complete the manufacturing process. Two and a half-inch aluminum bar stock was used to manufacture a cylinder measuring 25.00" in length, 2.145" at the right end, and 2.130" at the left end, with a linear taper from one end to the other.

The first challenge encountered in making this tool was center-drilling and tapping the ends of the part. This was done because the stock size exceeded the capabilities of the available machine tools

at CU Denver's Hub. Due to its length of 25", the stock extends beyond the available Z- height of the vertical milling machines. As a result, clamping the piece upright and milling it was not acceptable. Its diameter of 2.5" exceeded the throat of all three lathes, so turning the part was also not an option for the drilling and tapping. The horizontal milling head attachment for the manual mill is unfortunately of a Bridgeport design, which was unusable. In addition, the hub's Vextrax mill was unable to accommodate the part in its standard configuration. It was determined that utilizing the rotating head of the Vextracks mill would allow for the converting of the mill to accomplish the drilling. As a result of the limitations of the hub's other machines, the re-posturing of the Vextrax was deemed to be the most effective method for the center-drilling and tapping of the motor mount.

Figure 48 - Horizontal Mill Set Up

As shown in Figure 48, the setup for the center-drilling required the extensive use of gage blocks to be in-line with the Z-axis of the Vextrax head. Initially step blocks were used to fixture the part, but they were ineffective at holding the cylinder steady and rigid because the threaded rods were installed in t-slots that had a center-to-center distance which was smaller than the diameter of the cylinder itself. In order to bypass this problem, special clamps were manufactured to hold the piece using t-slots that were appropriately spaced around the part, which can be seen in Figure 49.

Figure 49 - Fixturing for horizontal milling

Given the fixturing for the horizontal milling, there is risk of lower accuracy than what would typically be expected. The gage blocks used in the setup were all measured to be the same height with digital calipers. Upon measuring the height of each stack, it was determined that there was a 0.003" difference from one side to the other, compromising accuracy by a relatively small margin. In addition, the milling head was leveled using a dial-indicator clamped to the table, which resulted

in a flatness of 0.001 across the length of the quill. Although this was deemed as sufficient, it provided another potential source of inaccuracy within the chosen fixturing though not enough inaccuracy to warrant any other changes. Lastly, the workpiece was indicated in two directions: the x-direction for squareness and the radial direction for concentricity. Each of these two indicating procedures had to be repeated on the second end of the piece and were, as expected, not entirely consistent with the first piece.

Despite the risks of poorer accuracy by using the Vextrax, the overall method proved to be more effective than initially anticipated. ½-13 threads were drilled and tapped on each end with a total indicator runout of 40 thousandths at its height, a potential difference of 0.080" from hole-center to hole-center. This inconsistency was of little consequence when the mandrel was turned with the SL-X lathe. However, this would only prove to be slightly problematic when installed on the X-winder.

Figure 50 - Finished Motor Mount Mandrel (Side)

Once the ends were complete and ready for turning, the part was turned between centers on the lathe to the specified diameters and tolerances and is now ready to be used for filament winding.

The next challenge in creating the motor mount was properly winding on the mandrel itself. In addition to the somewhat poorer accuracies from the center-drilling process, learning the intricacies of the X-winder proved a daunting task. As a start, a 4th-axis wind was conducted using the flat ends of the mandrel itself for the 'end winds'. This was done because, in theory, the winding angles could be made significantly smaller than it would otherwise. In reference to the mandrel's central axis, this method would have also yielded a greater tensile and compressive strength. This winding schedule was selected as the first approach based on the availability of the designer software.
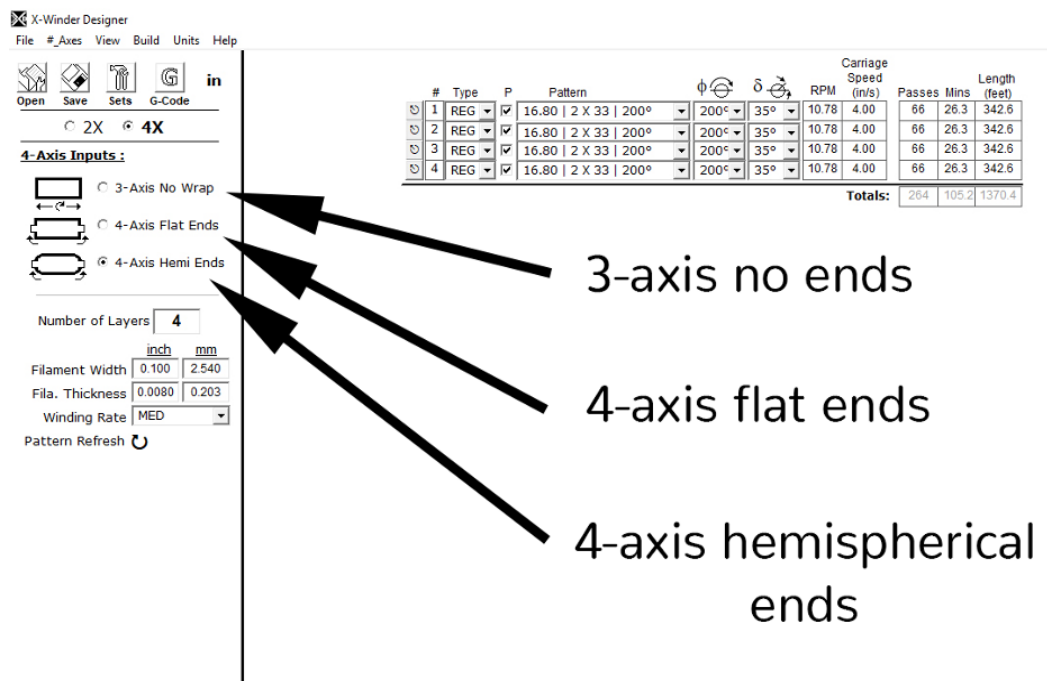

Figure 51 - X-Winder Designer Software Screen

Upon attempting this winding schedule with the flat ends, it was quickly discovered that the tension in the filament was significant, such that the flat ends with 90-degree edges would not be able to support the tension of the filament. This immediately resulted in slipping and misalignment of the filament, which would lead to the next design type, the 4-axis winding with hemispherical ends.

Multiple endcap profiles were manufactured and tested to examine their properties in relation to the mandrel design and X-winder's specifications, including a fully hemispherical design, one with a partial tangent radius, a fully hemispherical design with a flat face, and an elliptical. The results were dependent upon the correct path of the X-winder's delivery head. In addition, the filament placement on the end cap design also affected its effectiveness.
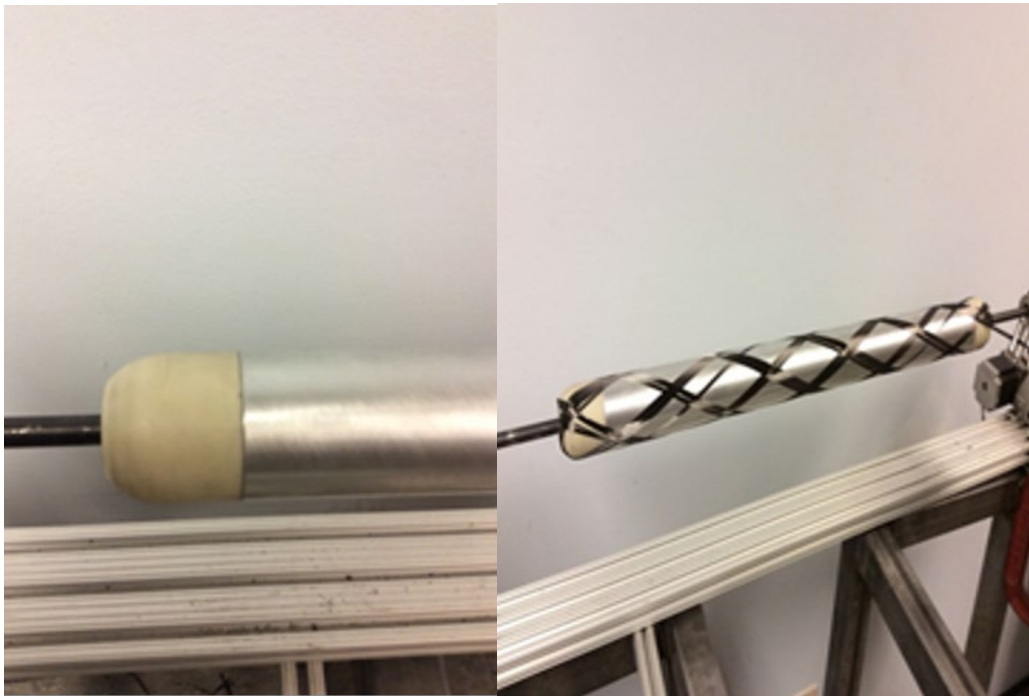

Figure 52 - Initial Endcap design (3), Hemisphere with Flats

One of the X-winder's many intricacies included the way the delivery head reacted to the runout of the mandrel, creating a number of challenges. Within each pass, the delivery head would collide with the mandrel's end caps, requiring a number of program optimizations. After several successful dry winds, it was decided to attempt a 'wet' wind, using the resin system.

Due to the issues mentioned earlier, the first wind using the resin yet was able to deliver some important results. Kevin Fornell was brought in as a liaison to assist *Polaris Rocketry* with the resin and filament design process, allowing for a demonstration of how the filament and epoxy mix resulted in a considerable loss of friction, which was of peculiar interest as the friction between the carbon fiber and the motor mandrel in the dry runs were not particularly high. This stressed the importance of the endcap design and the careful placement of the X-winder's delivery head path. In the end, the motor mount was successfully created.

Figure 53 - Motor Casing (Attached to Tool)

The wind featured above is constructed of 4 winds. Each wind contains 350 ft of carbon fiber filament totaling approximately 1400ft in this wind. The total mass of this part is .4938 lbm after removing the end caps and excess materials. This yields a fiber to matrix ratio of 49.9%.

Electronics Bay

Design

The electronics bay will be of a triangular prism design with 4-40 all-thread going through the edges of the prism. These threads will provide structural mounting points for the electronics bay and define its shape. Each face of the triangle will be 3D printed from PLA because it is relatively lightweight and strong enough for the purpose. The infill will be set to 15% since the walls are thin enough not to require much more from the infill of the printed piece. Holes will be drilled into each face of the prism to allow wires to be connected to each of the electronic devices and the batteries within the setup. The electronics will include one AltusMetrum EasyMini v2.0 altimeter and a TeleMega GPS and altimeter. They will be attached to the outer face of the prism where they will be easily accessible and allow for redundancy in the parachute deployment system. Two fiberglass bulkheads will be attached to each end of the prism. The forward bulkhead will have two cpvc cups that will hold and direct the blast of black powder charges. In addition to the cpvc cups on the forward end, there will also be an eye bolt for the main parachute. On the aft end of the electronics bay there will be an additional bulkhead attachment point and eye bolt as well as two more ejection cups for the second ejection set. This eye bolt will be the anchor point for the drogue parachute. When fully assembled the electronics bay will be six and a half inches long and have an outer diameter of 3.875". This will leave 1/16" on either side of the electronics bay for tolerancing and to allow for ease of removal.

An AltusMetrum EasyMini v2.0 was chosen as the primary altimeter for the rocket design, primarily because the device can support dual deployment launches like the ones that are expected at the Argonia Cup. The EasyMini is renowned for being, in essence, a self-programmable Particle Circuit Board (PCA) in which no remote control (RC) is required after launch. In addition, the barometric pressure sensor can support launches of up to 100,000 feet above sea level, which is far above what the *Polaris* rocket is expected to achieve. The design is also lightweight and compact, meaning that two of the 6.5 g devices can sit side-by-side on the electronics bay plate. In addition, the power requirements for the altimeter are also rather trivial, requiring only a 3.7-volt power supply. The altitude data could also be easily off-loaded using a USB cable and the device is also rather economical.

The AltusMetrum TeleMega v4.0 was chosen as the rocket's integrated GPS sensor and telemetry link. The device was ideal because it could support up to four configurable pyro channels and a 70 cm ham-band transceiver for a telemetry downlink. Like the EasyMini, it was designed to support dual deployment launches and support launches up to 100,000 ft above sea level while also being relatively compact and lightweight. The TeleMega was also an ideal fit as the rocket's GPS sensor because it could feed auxiliary data back to ground stations through VRF links. The device can store data onto its onboard computer while also providing real-time flight characteristic data to a host on the ground. The TeleMega's versatility makes it an ideal fit for the *Polaris* rocket.

Figure 54 - An Example of an Electronics Bay Section with an Altus Metrum TeleMega and EasyMini Side by Side.

Materials Selection

The rocket electronic bay is manufactured out of three main components which each use different materials. The main portion of the electronics bay will be made out of PETG which will be reinforced with threaded rods. On either end of the electronics bay will be a fiberglass bulkhead. Each bulkhead will house two separate ejection charge cups and e-matches as well as the mount for the parachutes. The ejection charge cups, made out of cpvc, will be used to hold the black powder charges on the end caps of the electronics bay. The cpvc is configured into a cup such that the rapid energy release caused by black powder combustion, will be directed out of the rocket body. This system will be held in place by one of the bulkheads which will be mounted to the upper airframe section. This glued hub will allow the remainder of the electronics bay to bolt on through nuts and washers such that the system does not move.

Manufacturing

The electronics bay for the rocket was first designed in Solidworks as a solid pyramid with no holes for electronics. After it was 3-D printed, using a 30% PLA infill, the component was drilled out to fit the electronics. This was done on the Vextrax mill. After securing the piece and tightening the base, a 3/64" drill bit was used to cut an initial hole that could be widened for wire pass throughs. The hole was widened to create a 1.5" x 0.25" rectangle that was 0.25" from the top of the part. Since this opening did not need to hold any parts no finishing cut was completed. After the wire pass through was created the remainder of the holes needed for the electronics were drilled and the components were mounted. At this point any rough edges were cleaned up and the part was made ready to be inserted into the main rocket body. The all-thread was then installed through the cavity on the PLA.

Once the main body of the electronics bay was completed the bulkheads previously manufactured were altered so that they fit the dimensions of the PLA. Since the 3-D printer used does not have tight tolerances this was done as a post processing step. Now that all the parts are fit to one another they were marked to indicate final positioning and glued into place on the rocket body. The electronics bay will be fully installed on the launch pad due to the finite battery life, and thus is removable. The final mechanical assembly can be seen in the figure below.
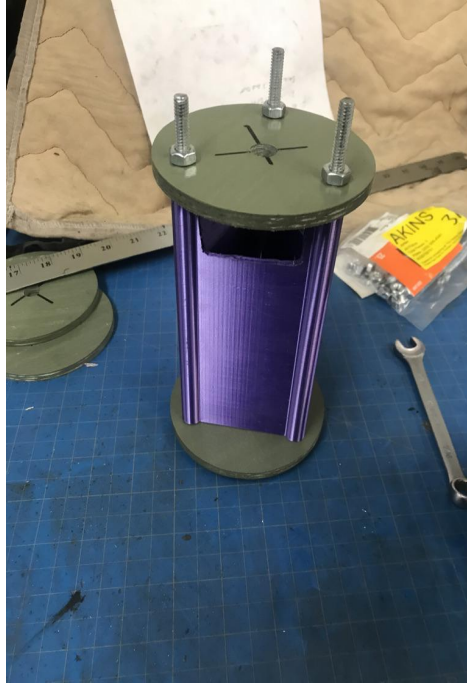
Figure 55 - Mechanical E-Bay

The Argonia Cup Competition Results

The Polaris Rocketry team successfully flew their rocket, which was made and designed in house, during the afternoon of August 27th, 2021. During the competition the team was able to complete all the required safety pre-checks and pre-flight preparations required by the Argonia Cup staff and then launch their vehicle. Once the pre-checks and safety checks were completed the rocket was launched and successfully recovered. Although the vehicle did not perform to the level it was expected to, the airframe and internal components did not experience any failures due to design. Upon review of the footage taken during launch and ascent it was noted that the rocket began a slight westward veer. When this happened, the rocket attempted to correct itself to a dynamic equilibrium at which point the vehicle became too unstable for sustained flight. Further review of the footage showed that, due to the unexpected changes in dynamic pressure and the abnormal flight pattern, the ejection charges for the parachutes deployed. This was confirmed upon review of the flight data taken by the on board and redundant EasyMini and TeleMega systems. After the ejection charges deployed the non-motorized portions of the vehicle continued in their

parabolic trajectory. The portion of the vehicle, which was still under load from the motor, which continued to burn until fuel starvation, continued the trajectory imposed by the motor and then proceeded to free fall to its final destination where it was recovered.

Gantt Chart

Polaris Rocketry Gantt Chart

Brendon Vu, Jordan Akins, Nicholas Diamond, Joshua Lucero, Jonathan Smith, Luna Sawaged, Clarke Dunn

University of Colorado Denver

| | Project Start Date | | 8/17/2020 (Monday) | | | Display Week | 27 |

	TASK	Responsibility	Day	Hours Required	Start Date	Due Date	DAYS	%
1	**High Priority Tasks**					-		
1.1	Plywood Bulkheads	Brendon		1.5	Sat 2/13/21	Sun 2/21/21	8	100%
1.2	Centering Rings	Brendon		1.5	Sat 2/13/21	Sun 2/21/21	8	100%
1.3	Drone Short Tabs	Nick, Luna, Jordan		6	Sat 2/13/21	Sun 2/21/21	8	100%
1.4	Nosecone Tip	Nick, Christian		4	Sat 2/13/21	Sun 2/21/21	8	100%
1.5	Drone Pins and Springs	Clark, Jordan		2	Sat 2/13/21	Sun 2/21/21	8	75%
1.6	Drone Arms x4	Nick, Jordan		8	Sat 2/13/21	Sun 2/28/21	15	100%
1.7	Fin Slots x3	Nick, Jordan		8	Mon 2/22/21	Sun 2/28/21	6	100%
1.8	Square Body Tubes	Nick, Christian		6	Mon 2/22/21	Sun 2/28/21	6	100%
1.9	Rocket E-Bay	Nick, Jonathon		10	Mon 2/22/21	Tue 3/02/21	8	50%
2	Fins x3	Nick, Brendon, Christian		5	Mon 3/01/21	Sun 3/07/21	6	100%
2.1	Polaris Video	Brendon		4	Mon 3/01/21	Sun 3/07/21	6	100%
2.2	Sand Body Tubes	Nick, Christian		8	Mon 3/01/21	Sun 3/07/21	6	100%
2.3	Motor Retainer	Nick, Luna		6	Mon 3/01/21	Sun 3/07/21	6	0%
2.4	Ejection Charges	Brendon, Jordan		10	Mon 3/08/21	Sun 3/14/21	6	0%
2.5	Midterm Report	All		20	Mon 3/08/21	Wed 3/17/21	9	5%
2.6	Fit and Assemble	All		10	Mon 3/08/21	Sun 3/21/21	13	10%
2.7	Final Solidworks Model	Jordan		1	Mon 3/08/21	Fri 3/26/21	18	50%
2.8	Final Open Rocket Model	Jordan		1	Mon 3/08/21	Fri 3/26/21	18	50%
3	COMPETITION	All		112	Mon 3/01/21	Fri 3/26/21	25	0%

Budget

Items to Procure

Glue	2	$69.00	$138.00	For centering rings, bulkheads, and motor mount
Travel	1	$500.00	$500.00	Hotel, Gas, and Food for 7 people
Aluminum Mandrel	2	$78.63	$157.26	To create a form that the body tube will wrap around during manufacturing. 6 foot sections
Threaded rods	1	$5.58	$5.58	For electronics bay inner tube
RF Controller	1	$300.00	$300.00	To guide the payload section to the target.
Altus Metrum	1	$516.60	$516.60	Two EasyMini v2.0, One TeleMega v4.0, Two Circuit Barrier Terminals, Two Rotary Switches
Total:			$3,646.96	Includes Payload

Payload				
Item	Quantity	Cost Per Item	Total Cost	Notes
PLA	1	52	$52.00	For payload body and propellers.
ARDUINO	1	$22.00	$22.00	"Brain"
Motor	1	$33.99	$33.99	Brushless motors for the propellers
ESC	1	$26.99	$26.99	Electronic Stability Control
Motor Control	1	$9.59	$9.59	Power Control Module
Battery	1	$18.99	$18.99	System power supply
IMU	1	$4.99	$4.99	Stability control component
Propellers	1	$15.99	$15.99	COTS alternative parts
Antenna	1	$15.99	$15.99	Transmission module for radio control
Total (Payload):			$200.53	

Budget Status as of December 1st, 2020

Items Procured		Budget	
Aluminum Tubes	$175.00	Starting Budget	$2,100.00
L1000W Motor	$317.03	OAI Donations	$600.00
Altus Metrum Electronics	$516.60	Twitch Donations	$1,000.00
Total:	$1,0008.63	Total:	$3,700.00

Recommendations & Conclusions

The Argonia Cup competition was a learning experience in ways that the Polaris team had not anticipated. Despite not winning the competition, the Polaris Rocketry team is proud of the illustrious work and effort that had been put into making a rocket entirely from scratch and flying it. It should be noted that the Polaris design was the only rocket of its class in the competition to be made entirely from scratch. However, should the team be given the opportunity to undertake such an endeavor again, several changes would have to be made in order to provide a higher likelihood of a successful launch. These changes include updating the flight simulations more rigorously, conducting a test-flight during competition, manufacturing a separate electronics bay section that is independent of the rocket, and some improvements to the payload section.

The first and arguably the most important lesson drawn, was that each component manufactured should have had its mass taken and inputted into the OpenRocket simulation regularly in order to ensure that the stability factors that were initially projected are indeed accurate. In line with the first lesson, conducting a flight test with a mock-payload section with another L1000 motor before the competition would have given the team some critical early warning of any potential issues that were experienced with the EasyMini, TeleMega, payload sections, and stability of the launch. Although it takes a significant amount of time to plan and conduct such a test, in addition to the time that would have been required to repair and diagnose any issues with the rocket, the information that would have been gained before the competition would have been invaluable. While this would not have been feasible for this year's team to complete, next years team should have more of an opportunity to do so given the knowledge they will receive from the provided data.

Although not necessarily to the mission objectives, a much-needed design change for any future rockets would include a separate electronics bay section. Due to a lack of experience and knowledge, it was decided that the electronics bay would not be manufactured within a separate coupler section that would join the nose cone and body section of the rocket. Rather, an electronics bay that was a part of the rocket itself would provide a simpler and more cohesive design with less parts. The decision was made to simply place

the electronics bay against the lowermost bulkhead on the upper airframe section, thus eliminating the need to manufacture and sand down more coupler and airframe sections on X-winder. Although this proved to be strategically useful in meeting our completion deadline, it proved to be tactically difficult on the day of the competition. The time and effort to refit the electronics bay section into the rocket each time it had to be removed was difficult and time consuming. Providing a separate system which is more accessible pre- and post-flight would allow for this process to be more streamlined and reduce the likelihood of error.

With regard to the payload and payload delivery sections, it is difficult to provide conjecture as to possible improvements. This section as a whole could have used a significant amount more time and manufacturing effort throughout the entire year. This section in and of itself is an entire project and needed that level of time and energy. Although significant time was put into the payload section, the focus of the team was mostly on manufacturing and designing the rocket itself. Given this information, changes to the deployment of the drone could have been made. For example, a system which allows for a drone that does not have articulable arms and rather has a sabot style casing which deploys a smaller profile drone would be preferable. Such a system would allow for the drone to reduce complexity greatly and possibly achieve stability much faster. The team does not have all the details surrounding such a design, however, it could greatly improve the probability of a zero issue flight and therefore, a competition win.

In addition to the preflight verification data and modifying the electronics bay design, modifications to the airframe couplers would be made. Although these components did not impede the rocket's performance on competition day, improvements could be made. Making the couplers thicker during their initial wind would provide more leniency for the rocket in the event of transverse stresses such as wind shear layers or inflight instability. This is also keeping in mind the overall rocket weight and dimensions, therefore minimizing internal volume losses, which could be used for additional payload improvements or electronic bay modifications.

Finally, the last major change to this year's rocket would be the motor selected. Within the scope of motors available to purchase in the L2 range, two main categories are available, that is; re-loadable and single use motors. This year chose to use a single use motor as these motors reduce the complexity of the motor mounting system and thus aid in maintaining a stable rocket. If given the opportunity to re-select a motor the team would opt for the, more complex, re-loadable system. This would expand the available motors greatly and, given the knowledge that the team possess post flight, would not greatly impede the manufacturability of the rocket in a significant manner. These changes would allow the team to achieve a greater factor of safety with regard to overall rocket capable altitude. In preliminary simulations, which have not been researched thoroughly, a similar rocket to this year, but with a different motor, could achieve approximately 10,000 ft AGL as opposed to the expected 8,500 ft AGL of this motor. Thus providing a greater margin of error and allowing the rocket to be slightly heavier if need be.

Despite these proposed changes it should be reiterated that the team is proud of the work that was accomplished, especially given the development research and production capabilities that the team needed to pioneer so that the project could be completed. The team learned a great deal outside of rocket- and drone-building itself, such as team cohesion, the leveraging of all-aspect integration, and mitigative risk aversion.
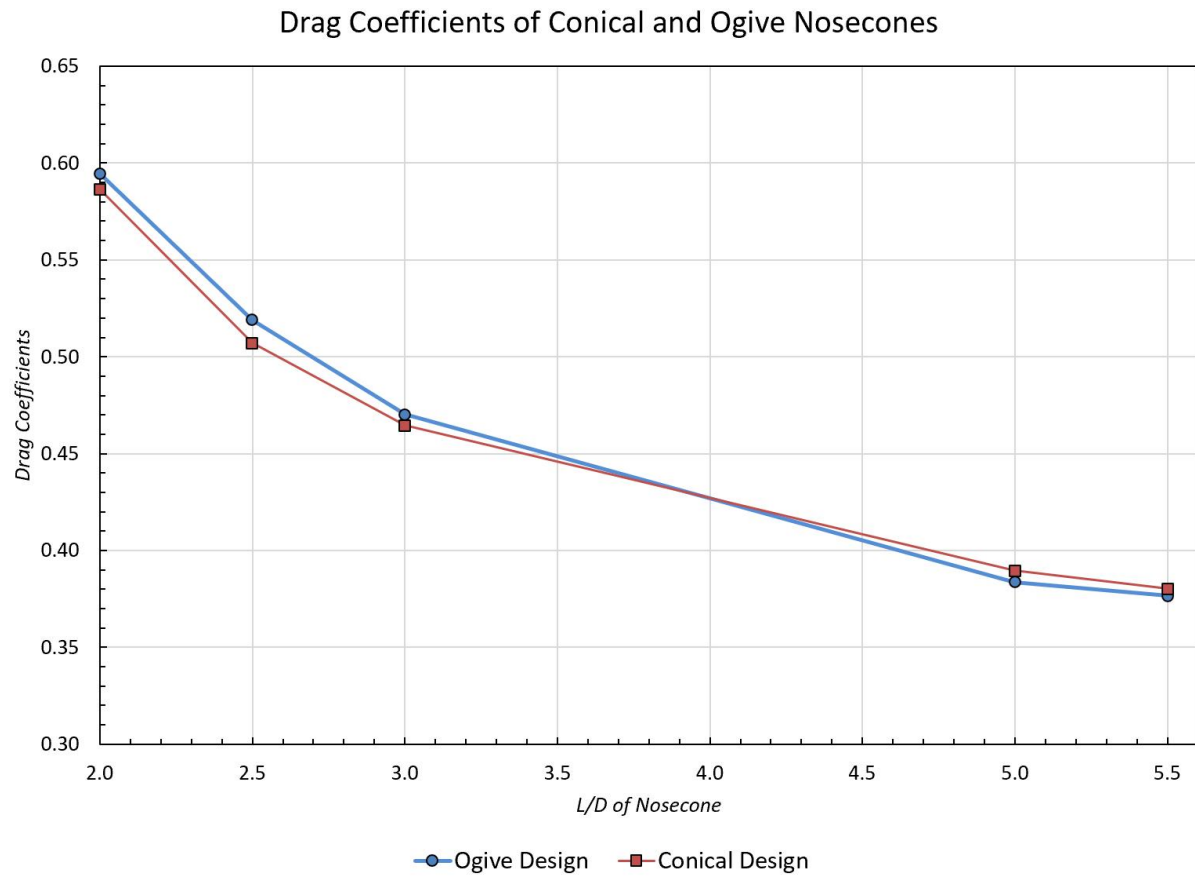
Appendices
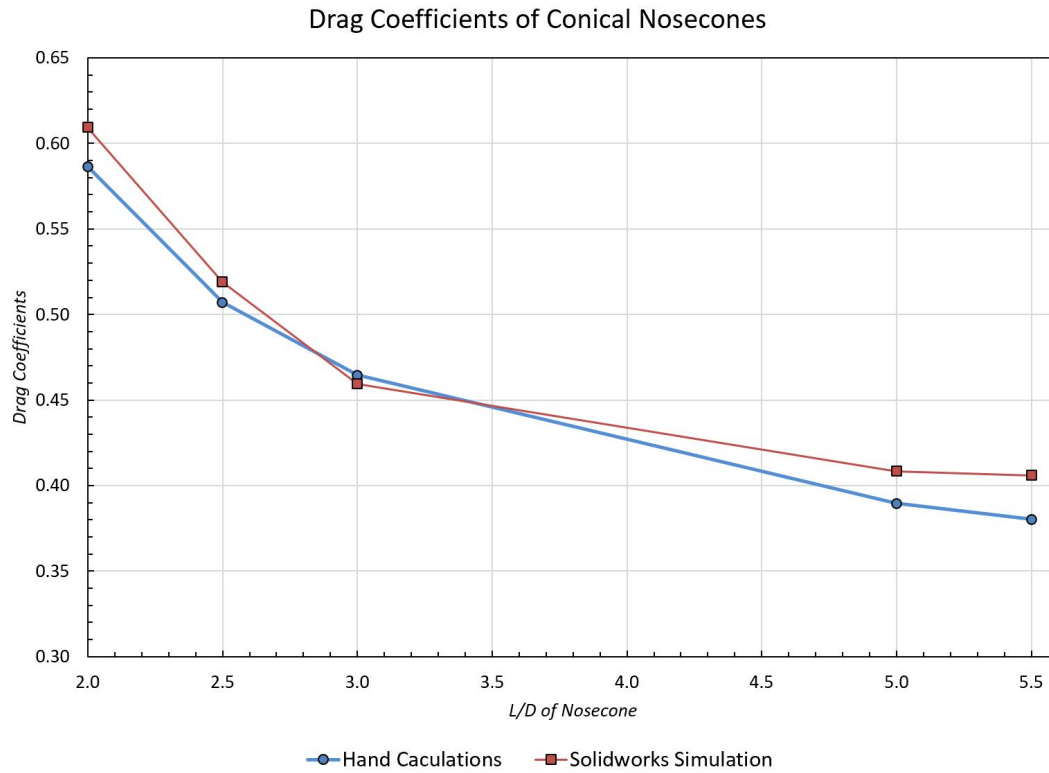
Appendix A: Drag Coefficient Results of Conical Nosecones for both Solidworks Simulations and hand-calculations.

Drag Coefficients of Ogive Nosecones
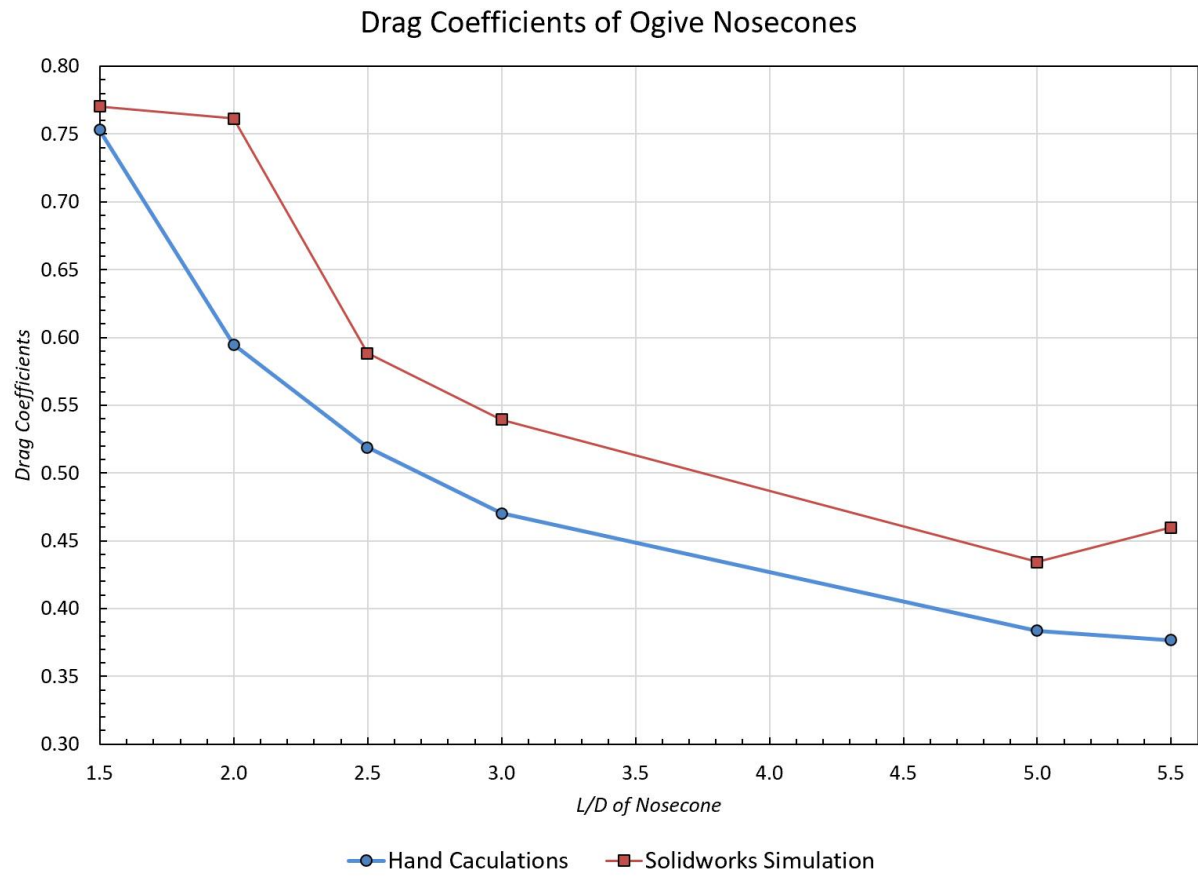
Appendix B: Drag Coefficient Results of Ogive Nosecones for both Solidworks Simulations and hand-calculations.
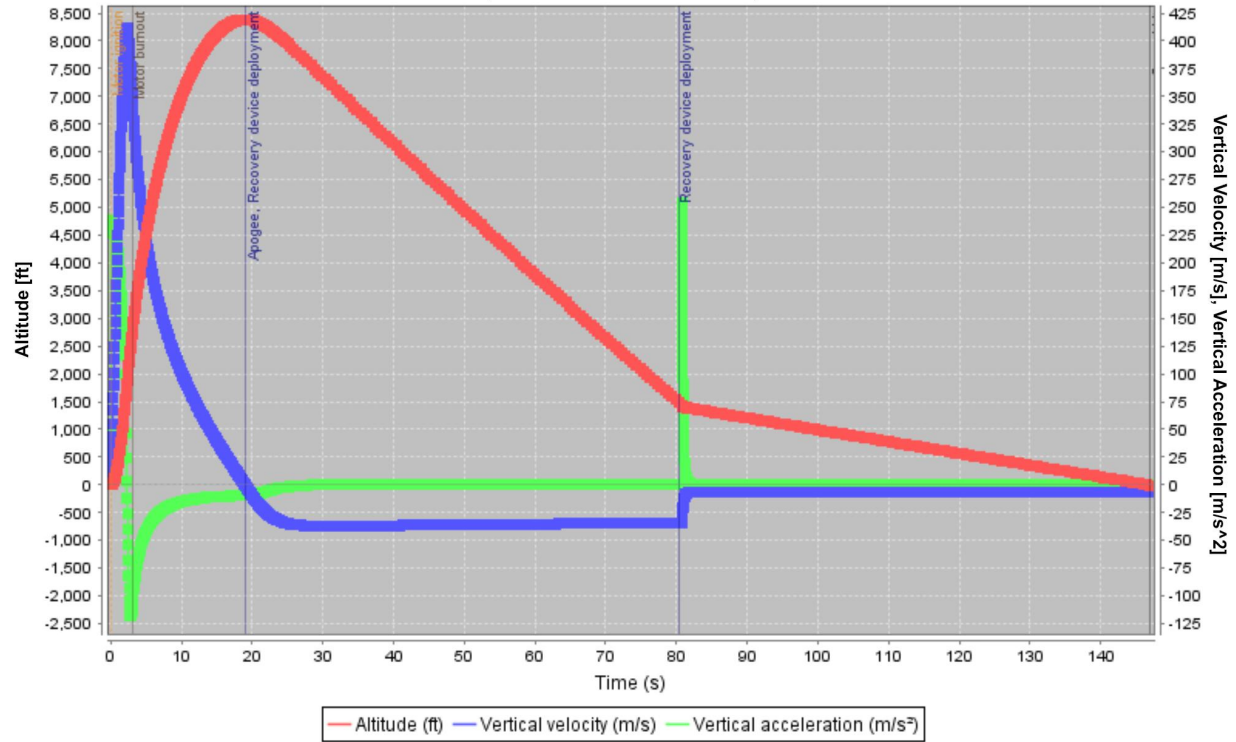
Drag Coefficients of Conical and Ogive Nosecones

Appendix C: Hand-calculated Drag Coefficients for Conical and Ogive designs for various

calibers of length.

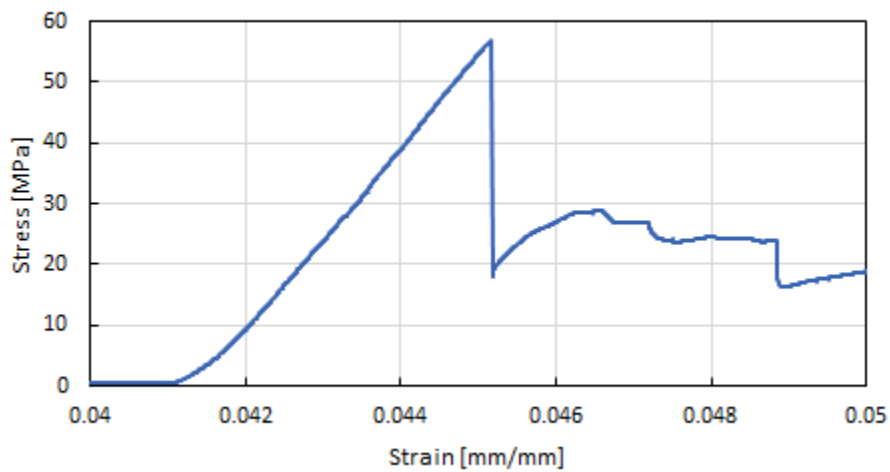**5-caliber Ogive Nosecone Flight Simulation Results**
(Vertical motion vs time)
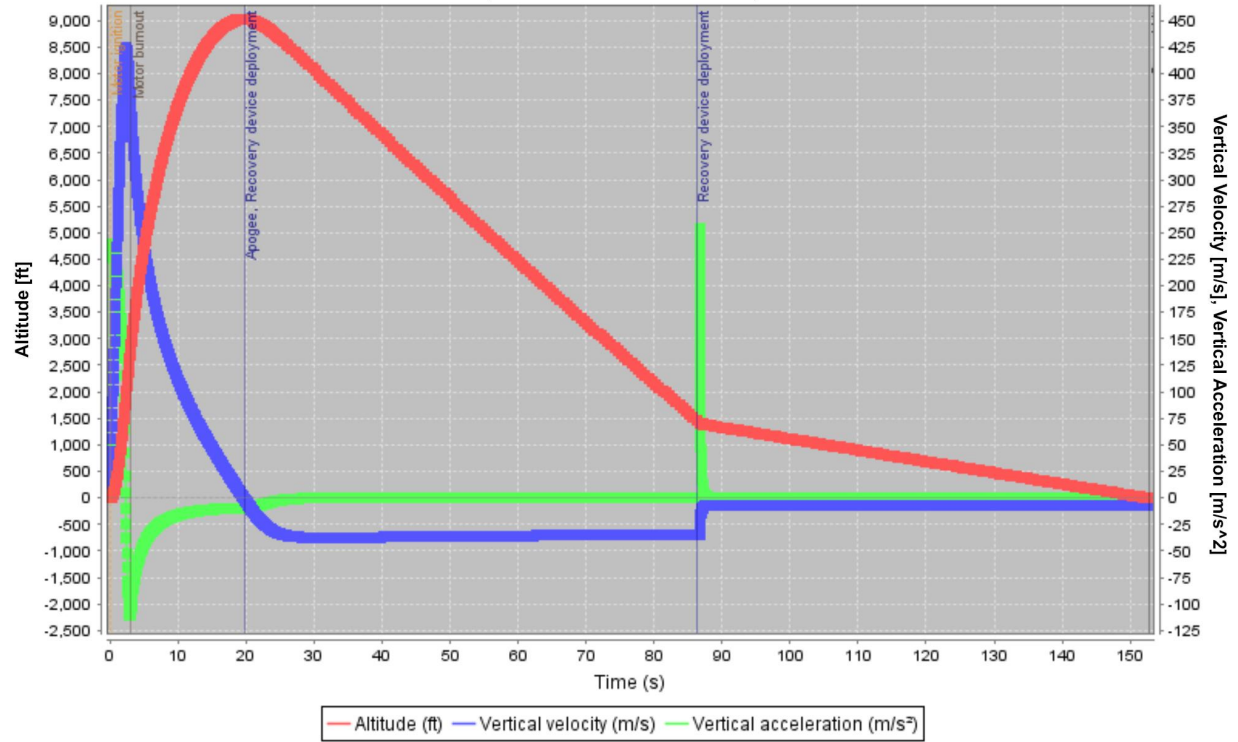
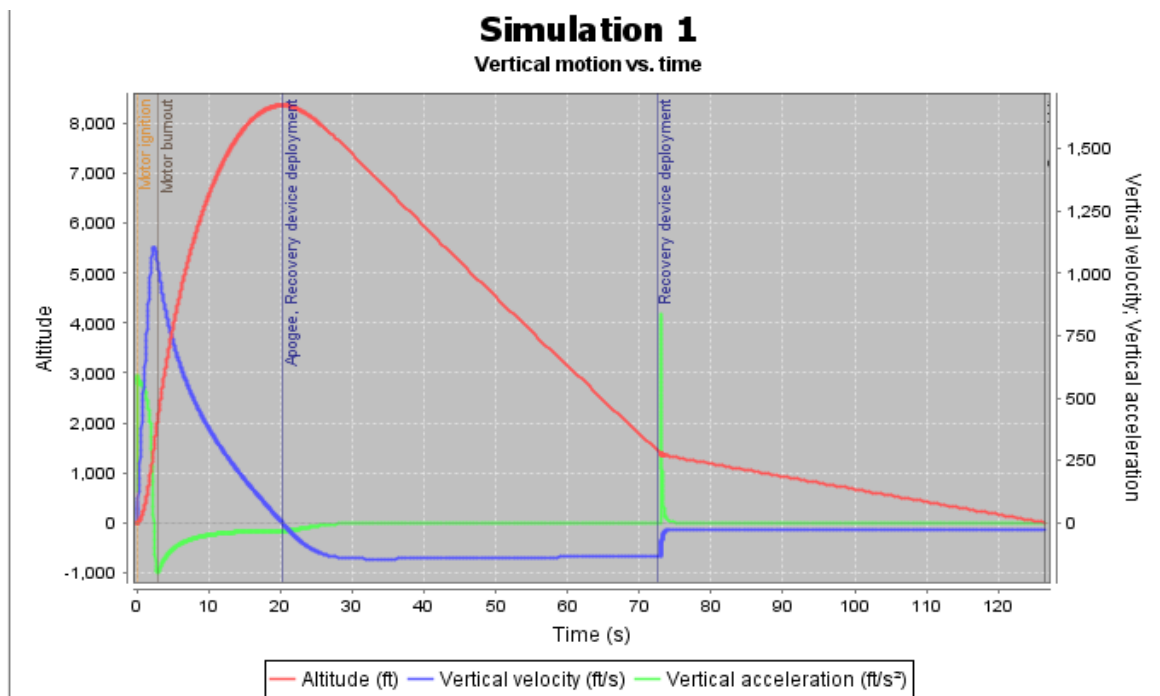Appendix D: Projected flight profile of a 5-caliber conical nose cone

Appendix E: Projected flight profile of a 5-caliber ogive nose cone

Appendix F: Derived Stress-Strain Results for Airframe Section 7104

Strain-Stress Results for Airframe Section 7107
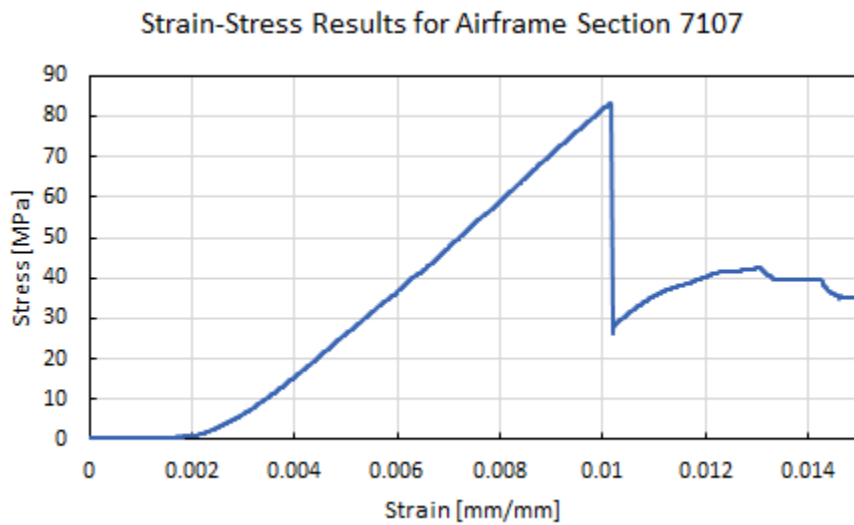
Appendix G: Derived Stress-Strain Results for Airframe Section 7107

Simulation 1
Vertical motion vs. time

Appendix H: Updated Flight Simulation

A. Glossary of Terms

    a. CFD - Computational Fluid Dynamics

    b. CG - Center of Gravity

    c. CP - Center of Pressure

    d. AGL - Above Ground Level

    e. ESC - Electronic Stability Control

    f. BEC - Battery Eliminator Circuit

    g. COTS - Commercial Off The Shelf